NASA TECHNICAL NOTE

NASA TN D-8490

NASA TN D-8490

EXPERIMENTAL PERFORMANCE OF AN ABLATIVE MATERIAL AS AN EXTERNAL INSULATOR FOR A HYPERSONIC RESEARCH AIRCRAFT

Richard L. Puster and Andrew J. Chapman

Langley Research Center
Hampton, Va. 23665

NATIONAL AERONAUTICS AND SPACE ADMINISTRATION • WASHINGTON, D. C. • NOVEMBER 1977

1. Report No.	2. Government Accession No.	3. Recipient's Catalog No.
NASA TN D-8490		

4. Title and Subtitle	5. Report Date
EXPERIMENTAL PERFORMANCE OF AN ABLATIVE MATERIAL AS AN EXTERNAL INSULATOR FOR A HYPERSONIC RESEARCH AIRCRAFT	6. Performing Organization Code November 1977

7. Author(s)	8. Performing Organization Report No.
Richard L. Puster and Andrew J. Chapman	L-11148

9. Performing Organization Name and Address	10. Work Unit No.
NASA Langley Research Center Hampton, VA 23665	516-56-01-02
	11. Contract or Grant No.
12. Sponsoring Agency Name and Address	13. Type of Report and Period Covered
National Aeronautics and Space Administration Washington, DC 20546	Technical Note
	14. Sponsoring Agency Code

15. Supplementary Notes

16. Abstract

An ablative material composed of silica-filled elastomeric silicone was tested to evaluate its thermal and structural performance as an external insulator, or heat shield, for a hypersonic research aircraft. The material was also tested to determine whether it would form a durable char layer when initially heated and thereafter function primarily as an insulator with little further pyrolysis or char removal. Aerothermal tests were representative of nominal Mach 6 cruise conditions of the aircraft, and additional tests were representative of Mach 8 cruise and interference heating conditions. Radiant heating tests were used to simulate the complete nominal Mach 6 surface-temperature history. The silica char that formed during aerothermal tests was not durable. The char experienced a general and preferential surface recession, with the primary mechanism for char removal being erosion. Tests revealed that radiant heating is not a valid technique for simulating aerodynamic heating of the material.

17. Key Words (Suggested by Author(s))	18. Distribution Statement
Ablative material Silica char Hypersonic research aircraft	Unclassified - Unlimited Subject Category 18

19. Security Classif. (of this report)	20. Security Classif. (of this page)	21. No. of Pages	22. Price*
Unclassified	Unclassified	45	$4.00

* For sale by the National Technical Information Service, Springfield, Virginia 22161

EXPERIMENTAL PERFORMANCE OF AN ABLATIVE MATERIAL AS AN EXTERNAL INSULATOR FOR A HYPERSONIC RESEARCH AIRCRAFT

Richard L. Puster and Andrew J. Chapman
Langley Research Center

SUMMARY

An ablative material composed of silica-filled elastomeric silicone was tested to evaluate its thermal and structural performance as an external insulator, or heat shield, for a hypersonic research aircraft. The material was also tested to determine whether it would form a durable char layer when initially heated and thereafter function primarily as an insulator with little further pyrolysis or char removal. Aerothermal tests were representative of nominal Mach 6 cruise conditions of the aircraft, and additional tests were representative of Mach 8 cruise and interference heating conditions. Radiant heating tests were used to simulate the complete nominal Mach 6 surface-temperature history. The silica char that formed during aerothermal tests was not durable. The char experienced a general and preferential surface recession, with the primary mechanism for char removal being erosion. Tests revealed that radiant heating is not a valid technique for simulating aerodynamic heating of the material.

INTRODUCTION

The National Aeronautics and Space Administration and the U.S. Air Force have conducted a joint study to define a hypersonic research aircraft (ref. 1). Minimum performance requirements for this vehicle include Mach 6 cruise sustained for 40 seconds at an altitude of 27 to 30 km (88 600 to 98 400 ft). A possible vehicle configuration and a nominal Mach 6 flight trajectory are shown in figure 1. The resulting aerothermal flight conditions during the cruise portion of the trajectory are presented in table I for the nominal Mach 6 flight as well as for flight to Mach 7 and 8. The aerodynamic heat load for this vehicle poses structural and material problems which must be resolved in the design of the vehicle. One approach being considered is the use of a conventional aluminum structure protected by an ablative insulative material (SLA-220) bonded to the outer surface (refs. 2 and 3). SLA-220 material is a silica-filled elastomeric silicone which has been proposed as an external insulator, or heat shield, on the basis of its predicted ability to pyrolyze and form a durable char layer during initial exposure to aerodynamic heating, and thereafter to function primarily as an insulator with little further pyrolysis and essentially no char removal. The suitability of SLA-220 as a heat shield for a hypersonic research aircraft is dependent upon its ability to perform in this mode.

The present investigation was carried out to evaluate the thermal and structural performance of SLA-220 and to verify the predicted performance mode stated above. Three panels, consisting of SLA-220 bonded to aluminum substrate panels, were tested in the Langley 8-foot high-temperature structures tunnel during repeated aerothermal cycles at test conditions representative of the nominal Mach 6 cruise conditions, and at additional, more severe test conditions representative of the Mach 8 cruise or interference heating conditions. Tests were made with the SLA-220 molded in two different configurations and in two different lengths. The total heat load of these aerothermal tests was about one-half that of the entire flight trajectory. To evaluate performance of the SLA-220 when subjected to the entire flight heat load, one panel was exposed to radiant heating, which simulated surface temperatures for the 600-second Mach 6 flight trajectory.

SYMBOLS

Values of physical quantities are given in the International System of Units (SI) and in U.S. Customary Units. Measurements and calculations were made in U.S. Customary Units. Conversion factors relating the two systems are given in reference 4.

ℓ	panel length, m (in.)
T	temperature, K (^{o}R)
TPS	thermal protection system
t	exposure time, s
U	velocity, m/s (ft/sec)
x,y,z	panel-holder coordinates, m (in.) (see fig. 4)
x_p,y_p,z_p	panel coordinates, m (in.) (see fig. 3)
δ	boundary-layer thickness, m (in.)

Subscript:

e	edge of boundary layer

APPARATUS

Test Material and Panels

The material evaluated was a silica-filled elastomeric silicone with an average density of 240 kg/m^3 (15 lb/ft^3). The silica is primarily microspheres, with a lesser amount of the silica being in the form of short fibers. This material, designated SLA-220 by the manufacturer, is described in references 2 and 3. The material was fabricated to form two different configurations, stri-

ated and reinforced. The striated test material had cuts to one-half the material thickness in a 1.27-cm (0.5-in.) square grid pattern. The purpose of the striations was to relieve thermal stresses which occur during pyrolysis and to allow for material shrinkage. The striated material has a density of 224 kg/m^3 (14 lb/ft^3). The reinforced material was molded into small cells by a glass fiber and polymer resin honeycomb structure. The partitioning of the material by the honeycomb walls serves the same function as the striations in the first configuration; in addition, the honeycomb structure is intended to help maintain char integrity. The reinforced material had a density of 256 kg/m^3 (16 lb/ft^3).

Test panel 1 (fig. 2) and test panel 2 consisted of four 25.4-cm (10.0-in.) square quadrants of the test material, 1.52 cm (0.60 in.) thick, bonded to 50.8-cm (20.0-in.) square stiffened carrier panels. The carrier panels were fabricated from sheets of 2024 aluminum 0.127 cm (0.050 in.) thick. A sketch of test panels 1 and 2 is shown in figure 3(a). The stiffness and mass of the carrier panels are representative of aircraft structure. The two material sections on the left half of panel 1 were composed of the reinforced material, and the two sections on the right half of panel 1 were composed of the striated material. On panel 2 the two test materials were applied alternately to each side, as shown in figure 3(a). Test panel 3, shown in figure 3(b), was composed of the striated material; the length, width, and depth of the material were, respectively, 84.6 cm (33.3 in.), 50.8 cm (20.0 in.), and 1.27 cm (0.50 in.). The aluminum substrate was relatively thick, 0.24 cm 0.094 in.), although the effective thermal capacitance of the thick plate was the same as that of the carrier plate and stiffeners of the other two panels.

Panel Holder

Test panels were mounted in the panel holder (figs. 4 and 5) for testing in the Langley 8-foot high-temperature structures tunnel. The panel holder was a rectangular slab with a sharp leading edge, in the plane of the top surface, which was faired to the lower surface by a 20° bevel. A spanwise row of metal spheres on the upper surface, parallel to and 12.7 cm (5.00 in.) aft of the leading edge, tripped the boundary layer to insure uniform turbulent flow over the test surface. Aerodynamic fences were used on tests of panels 1 and 2 to provide parallel flow over the surface of the panel holder. The test panels were mounted in openings on the surface of the panel holder at the positions shown in figure 4. Test panel 1 can also be seen in figure 5. The test-panel surfaces were flush with the surrounding panel-holder surface, which was covered with high-density Glasrock. The local flow and aerodynamic heat flux on the panel holder have been calibrated, and these results are reported in reference 5.

Instrumentation

Test panels 1 and 2 were instrumented with thermocouples to measure the temperature of the ablative material and the aluminum carrier plate. Thermocouple installation details and locations are shown in figure 6. Six thermocouples were installed in the test material in plugs inserted from the back of

the panel so that the thermocouples were 0.32 cm (0.125 in.) from the surface. Ten thermocouples were attached to the aluminum substrate as shown in figure 6.

Surface temperatures were measured by a scanning infrared radiometer for test panel 2. An area of 5040 cm^2 (781 in^2) is mechanically scanned by the infrared radiometer with a spatial resolution of 1.3 cm (0.52 in.) in diameter. About 5 seconds is required to scan the entire area. The data are recorded on an FM system, digitized, and then plotted. This system operates at a wavelength of 2.4 μm to avoid absorption bands of carbon dioxide and water vapor present in the test medium.

A survey probe (fig. 7), comprised of a pitot pressure probe and a total temperature probe, was used to measure the flow above the surface of the test panel and was located just ahead of test panels 1 and 2 (fig. 4). The probe was flush with the surface of the panel holder when not in use. The static pressure was measured from orifices flush with the panel holder, as shown in figure 4, and was assumed to be invariant throughout the boundary layer. With total temperature, pitot pressure, and static pressure measured as a function of distance normal to the panel surface, the equations and procedures given in reference 6 were used to calculate boundary-layer parameters of interest.

Facility

Tests were performed in the Langley 8-foot high-temperature structures tunnel, a hypersonic blowdown wind tunnel. The high-energy test stream consists of the products of combustion obtained from a mixture of methane and air burned under pressure in a plenum chamber. The flow is expanded through an axisymmetric, contoured nozzle to approximately Mach 7 into an open-jet test section. The flow is decelerated in a supersonic diffuser, pumped through a mixing tube, and exhausted into the atmosphere by a single-stage annular air ejector. A schematic of the facility is shown in figure 8. The panel holder is stowed in the pod below the test section prior to the establishment of hypersonic flow, as shown in figure 8, and is then rapidly inserted into the test stream after transient starting conditions have subsided and the desired flow has been established. As the panel holder moves from its stowed position it is simultaneously pitched to the angle of attack required for the test. The panel holder then moves through the test stream stopping at the center line. The panel holder with its aerodynamic fences can be used at angles of attack up to 15° without causing tunnel flow breakdown. Additional information about the facility may be found in reference 7.

Radiant heaters were used to simulate the heat load to the panels for an entire trajectory time of 600 seconds. The radiant heaters, located outside the wind tunnel and operated in air at ambient conditions, consist of quartz lamps with a total power capacity of 0.4 MW and an effective lamp area of 142 × 158 cm (56 × 62 in.). The maximum model size that can be tested is 108 × 152 cm (42.5 × 60 in.) with the test panel located from 10.2 cm (4 in.) to 20.4 cm (8 in.) from the quartz lamps.

TEST CONDITIONS

Most of the present tests were performed at conditions representative of the nominal Mach 6 cruise for about 40 seconds. An attempt was made to match the surface heat flux and shear stress for the reference location 254 cm (100 in.) from the nose of the hypersonic research aircraft. (See table I.) The test conditions required to simulate flight conditions were determined from the wind-tunnel and panel-holder calibrations of reference 5. A thermochemical equilibrium computer program (ACE) described in reference 8 was used to calculate the gas composition, and the thermodynamic, transport, and flow properties of the test medium. The gas composition is listed in table II for each test. The boundary-layer conditions on the panel-holder surface were calculated by using measurements from the boundary-layer survey probe. Additionally, the computer program of reference 9 was used to calculate theoretical boundary-layer properties, including the aerodynamic heat flux and shear stress, by using measured conditions as input. The pertinent parameters for each test panel are listed in table III.

During the tests on panel 1 (table III(a)) the aerodynamic heat flux was varied from 25 kW/m^2 (2.2 Btu/ft^2-sec) to 306 kW/m^2 (27.0 Btu/ft^2-sec), and shear stress was varied from 29.2 Pa (0.61 lb/ft^2) to 232 Pa (4.85 lb/ft^2). This range of conditions represents surface heat flux below, at, and above the nominal Mach 6 aerodynamic heat flux at the reference location 254 cm (100 in.) from the nose of the hypersonic research aircraft. (See fig. 1 and table I.) The higher or more severe aerodynamic heat-flux conditions could represent interference heating, or increased heat flux associated with flight at a lower altitude, higher angle of attack, or higher Mach number. The tests on panel 2 (table III(b)) and panel 3 (table III(c)) were at heat-flux and shear-stress levels representative of the reference location for the nominal Mach 6 cruise conditions except for the very short exposure during the last test (test 7) on panel 3; the aerodynamic heat-flux and shear-stress levels for this test were equivalent to those of test 10 on panel 1.

RESULTS AND DISCUSSION

Boundary-Layer Characterization

A typical boundary-layer velocity profile is presented in figure 9 for a panel-holder angle of attack of 7° for test 7 on test panel 2. The ratio of the local velocity to the velocity at the edge of the boundary layer U/U_e is plotted as a function of the ratio of the normal distance from the surface to the boundary-layer thickness y/δ. The experimental results, indicated by the symbols, are compared with the curves obtained using reference 9. For calculation of the experimental velocity, the Rayleigh equation with the measured static pressure at the surface, the pitot pressure, and the total temperature was used, and an isentropic relationship between static temperature and the measured total temperature was assumed. The boundary-layer thickness δ above the panel-holder surface was determined by the accepted criterion - local

velocity equal to 0.995 of the free-stream velocity above the panel-holder surface. The free-stream velocity had a maximum standard deviation of 0.008 of the mean velocity at a distance normal to the surface from 2.80 cm (1.10 in.) to 7.62 cm (3.00 in.) with a minimum of 15 data points. The experimental boundary-layer velocity profiles agreed with the predicted turbulent profile obtained by using reference 9. Similar comparisons for the other tests indicated that the boundary layer on the panel holder was fully turbulent for all tests.

Test Panel 1

Low aerodynamic heat flux.- The first 6 tests on panel 1 (table III(a)) represented the low aerodynamic heat flux and shear stress for the initial portion of a flight trajectory (ref. 1) or locations on the aircraft where the aerodynamic heat flux was below that of the nominal Mach 6 conditions of table I. During the first four tests, the maximum temperature measured by the embedded thermocouples of both the striated and reinforced SLA-220 was 575 K (1035° R); during the next two tests, the maximum temperature was 711 K (1280° R). The most noticeable change in the striated material after the first six tests was a slight opening of the striations because of material shrinkage from pyrolysis. The only visible change in the reinforced material was a darkening of the honeycomb cell walls.

Nominal aerodynamic heat flux.- The first significant change in the appearance of the test panel occurred during tests 7 and 8. (See table III(a).) Figure 10 shows the panel condition after these tests. The maximum temperature measured by the embedded thermocouples was 850 K (1530° R). The surface of the striated and reinforced SLA-220 pyrolyzed forming a silica char. The striated SLA-220 eroded slightly, producing wider striations with rounded edges in the flow direction, an effect which did not occur in the spanwise striations. The reinforced SLA-220 changed very little. Localized craters seen on the surface of the panel resulted from impingement by solid particles which originated in the tunnel combustion chamber.

Severe aerodynamic heat flux.- The next two tests (tests 9 and 10, table III(a)) were conducted at heat-flux levels greater than those of the nominal Mach 6 condition and comparable with the cruise heat flux of Mach 8 flight conditions at the dynamic pressure listed in table I. The aerodynamic shear-stress level in tests 9 and 10, however, is about 35 percent higher than that given in table I. The appearance of the panel after these tests is shown in figure 11. The striated SLA-220 eroded to a very noticeable and substantial extent, and the streamwise striations continued to widen. The reinforced SLA-220 has a rough irregular surface, and the material above the embedded thermocouples is absent.

The last two tests (tests 11 and 12, table III(a)) are representative of aerodynamic heat-flux and shear-stress levels anticipated in interference heating regions. The panel, after these tests, is shown in figure 12. The streamwise striations of the striated SLA-220 have eroded into channels which increase in width with test-panel length. In contrast, the spanwise striations show minimal erosion. The reinforced material was more resistant to erosion;

the erosion formed a regular pattern of shallow channels between honeycomb cell-wall intersections.

Posttest examination.- The posttest condition of the SLA-220 is shown in figure 13 by a series of spanwise-section photographs of test panel 1 illuminated by long-wavelength ultraviolet light. Ultraviolet light causes the char layer to appear fluorescent and allows it to be distinguished from the virgin material. Also, the char was identified by a difference in texture. In the reinforced material the additional fluorescence of the honeycomb is characteristic of the glass fiber/polymer resin material and does not indicate char formation. The char and its interface with the virgin material are typically labeled in figure 13(g). As indicated earlier, the striations increase in width from the leading edge to the trailing edge. Examination of figure 13 also shows that for both the striated and reinforced SLA-220 the surface has receded from the original surface (O.S.) position; the reinforced material appears to have less recession than the striated material. The surface recession and the char–virgin-material interface depth are plotted as a function of the streamwise panel length (x_p/ℓ) in figure 14. The thicknesses of the char and the virgin material are indicated. The distances plotted in figure 14 are averages of values measured from the middle two-thirds of the spanwise sections. The surface recession increased with panel length on both the striated and reinforced sections. This result was not expected since aerodynamic heat flux was predicted to decrease slightly with panel length. Although the surface was very rough (fig. 12) after the severe heat-flux tests, the measurements presented in figure 14 indicate that at $x_p/\ell = 0.9$ no more than 25 percent of the reinforced material and 33 percent of the striated material was affected. The overall surface recession was 11 percent for the reinforced material and 16 percent for the striated material. All percentages are relative to the original thickness of the material.

From the tests and data of test panel 1 some tentative observations can be made about the SLA-220. The material in both the striated and reinforced forms remained reasonably intact and protected the underlying aluminum structure from the hot hypersonic test stream under conditions ranging from below the nominal Mach 6 cruise conditions listed in table I to conditions far more severe than the reference conditions. The material pyrolyzed and formed a silica char; however, the char did not remain intact. Both SLA-220 configurations experienced general surface recession.

Test Panel 2

Nominal aerodynamic heat flux.- Repeated flight exposures of test panel 2 conducted at the nominal Mach 6 cruise conditions were used to evaluate the performance of SLA-220. A comparison of the conditions of this test, which are listed in table III(b), with table I flight conditions shows that almost all aerothermal parameters of significance were either duplicated or closely simulated. The appearance and condition of the panel after test 3, or 122 seconds of cruise flight exposure, are shown in figure 15 and are similar to the appearance and condition of panel 1 after test 8 (fig. 10). As before, numerous impact craters caused by solid particles from the tunnel combustor were

evident. The appearance and condition of the panel are very similar to those of panel 1 after exposure to the nominal Mach 6 cruise conditions.

Testing of panel 2 was terminated after nine test exposures so that the panel could be examined without further deterioration. Photographs of the panel following removal from the holder are shown in figure 16. The overall panel view in figure 16(a) shows localized craters, caused by particle impingement, and damaged thermocouple plugs in the reinforced sections. Figures 16(a) and 16(b) show that the longitudinal striations, as observed on panel 1, have eroded to narrow channels that increase in width with panel length. Figure 16(c) shows that shallow, wide channels between honeycomb cell-wall intersections were eroded on the surface of the reinforced material, which was more resistant to erosion than the striated material. The erosion through the striations of section 3, shown in figure 16(a), has cut short grooves into the reinforced material of section 4; conversely there is no appreciable effect of the reinforced material of section 1 on the downstream striated material of section 2. Under repeated exposure to the aerodynamic heat flux and shear stress of the nominal Mach 6 cruise conditions, panel 2 eroded and had a similar appearance to that of panel 1.

Panel temperatures.- The maximum temperatures of the material, measured by the embedded thermocouples 0.32 cm (0.125 in.) below the surface, varied from about 849 K (1528° R) during the first four tests to a maximum of about 889 K (1600° R) during the last five tests. The temperature increased slightly with each exposure. The maximum surface temperature of the material, as measured by the radiometer, was about 1000 K (1800° R) during the first four tests and about 1080 K (1944° R) during the last five tests. A surface-temperature relief map of test panel 2 during test 8 is shown in figure 17. The edges of the material were slightly hotter than most of the surface. The sharp temperature peaks represented local hot spots that were caused by recesses in the surface either from impacts or material loss over the thermocouples embedded in the material. The temperatures of the honeycomb-reinforced material were always 40 to 50 K (72° to 90° R) higher than those of the striated material. This temperature difference was probably due to differences in surface geometry, density, and total emissivity because of surface roughness.

Test Panel 3

Nominal aerodynamic heat flux.- To investigate further the previously observed effect of panel length, panel 3 was tested at the nominal Mach 6 cruise conditions. The combustion chamber was cleaned and overhauled to minimize sources of solid particles which impinged upon the surfaces of panels 1 and 2. Test conditions for panel 3 are given in table III(c).

After six tests and an aerothermal exposure time of 190 seconds, the condition of the panel was as shown in figure 18. The material exhibits characteristics similar to those of panel 2, although the level of the effects is less. The streamwise striations are wider than the spanwise striations and increase in width with panel length. Although not evident in figure 18, there is a slight recession of the material that increases with panel length. The

damage sites from impacting particles, principally iron oxides from the combustor, have been dramatically reduced but not eliminated.

The last test on panel 3 was under almost the same conditions as test 10 on panel 1. The test duration was short, only 15 seconds, since tunnel flow breakdown occurred in the test section. The panel is shown after the test in figure 19; damage to the SLA-220 from the abrupt pressure change was localized and limited primarily to the edges.

Posttest examination.- The posttest condition of the SLA-220 is shown in figure 20 by a series of spanwise-section photographs of panel 3 illuminated by long-wavelength ultraviolet light, which causes the char layer to appear fluorescent. Each photograph is identified by its distance from the leading edge of the panel. The striations increased in width from the leading edge to the trailing edge, although this effect is not as pronounced as it was on panel 1. (See fig. 13.) The char on panel 3 (fig. 20) is more uniform than that on panel 1 (fig. 13). This is probably because the test conditions for panel 3 were less severe; the test duration was shorter and the debris from the combustor was reduced. The surface recession and the char–virgin-material interface depth are plotted as a function of the streamwise length (x_p/ℓ) in figure 21. The thicknesses of the char and the virgin material are indicated. As mentioned previously, surface recesssion increased with panel length. The measurements presented in figure 21 indicate that at $x_p/\ell = 0.9$ about 27 percent of the SLA-220 was affected and the overall surface recession was about 5 percent. All measurements are relative to the original material thickness. Thus, the surface recession on panel 3 was about one-third that of the striated material of panel 1, although the percentages of material affected differ only slightly.

Erosion Mechanism

The mechanism for material removal, or surface recession, in these tests appears to be erosion caused by two main sources of solid particles: (1) debris from the tunnel combustion chamber and (2) silica char dislodged from upstream surfaces of the panel. The silica char, composed of silica microspheres held together with very fragile mechanical bonds, is a very significant source of erosion particles. The silica microspheres within the char could easily be dislodged by the multidirectional shear forces of a compressible turbulent boundary layer which scrub the exposed surfaces. Once free, the microspheres, as small as 30 μm (1.2 mils) in diameter, would be accelerated to velocities approaching the local velocity. Thus, the cloud of high-velocity silica particles would increase in particle density and become increasingly abrasive to the test panel as panel length increased.

The particulate densities from the two sources in these tests were evaluated for panel 3. After the first six tests of panel 3, there were about 1400 impact sites on the panel caused by particles from the combustor. Thus, there were about 17 impacts per second and a particle flux of about $43/m^2$-s ($4/ft^2$-sec). The size of these particles is unknown. The particle flux from the char impacting the surface was estimated to be $2.16 \times 10^9/m^2$-s ($2 \times 10^8/ft^2$-sec). This flux was determined from the measured recession, the

char composition, and the time-variant properties of the compressible turbulent boundary layer. The silica particle size varied from 30 to 125 μm (1.2 to 4.9 mils). It was concluded that in these tests the larger particles from the combustor caused discrete and random damage to the SLA-220 test panels. However, the silica particles from the SLA-220 char, which had a particle flux about 20×10^9 times that of the combustor particles, caused a uniform surface erosion of the test panel. The erosion was more pronounced in the streamwise striations, since the local flow probably attached to the sidewalls and the upper edges of the streamwise striations. Therefore, erosion from the high-velocity silica cloud would cause the streamwise striations in the SLA-220 to increase in width with time and panel length, and would cause the upper edges to become rounded. Eventually, the streamwise striations would become streamwise channels. The spanwise striations would not experience such a preferential erosion. The reinforced SLA-220 would also be subjected to such an abrasive mechanism; however, the intersection of the honeycomb cells is more resistant to the erosion which results in the formation of shallow channels between the honeycomb cell-wall intersections. Therefore, the proposition that the SLA-220 forms a durable char layer and performs primarily as an insulator was not demonstrated in tests at the nominal Mach 6 conditions.

Radiant Heating Tests

The aerodynamic tests simulated cruise heat flux but imposed a lower total heat load than predicted for the entire flight. Consequently, the aluminum carrier-plate temperatures did not reach the structural temperatures expected during flight. To evaluate the effects of a total flight heat load, test panel 2 was exposed to two radiant heating cycles which were programmed to simulate surface temperatures during flight. During the radiant heating tests, panel 2 was exposed to the surface-temperature history shown in figure 22. This temperature history is realistic for the nominal Mach 6 flight conditions. In figure 22 the surface temperature of the striated SLA-220 was measured by a radiometer. The temperature 0.3 cm (0.13 in.) below the surface and the temperature of the aluminum carrier plate were measured by thermocouples. The temperature of the aluminum carrier plate increased 147 K (265° R), which is close to the 167 K (300° R) predicted for the nominal Mach 6 flight conditions.

During another radiant heating test, the panel was inadvertently heated to a surface temperature of 1488 K (2678° R), which was nearly 400 K (720° R) higher than the maximum surface temperature predicted for flight. The carrier-plate temperature increased 257 K (463° R). The upper surface of the SLA-220 decomposed to form a chalky, rubbery residue. (See fig. 23.) The deposits were more pronounced along the upper edges of the honeycomb walls and in the striations than on other parts of the surface.

Photographs of a series of spanwise sections of test panel 2 illuminated by ultraviolet light are shown in figure 24. The radiant heating tests produced the dark layer, which did not occur in the material exposed only to convective heating. (Compare fig. 24 with fig. 13.) During the convective heating tests, pyrolysis occurred in a well-defined zone at the char–virgin-material interface, below which essentially no reactions occurred. Most of the carbon and hydrocarbon compounds produced by pyrolysis combined with oxygen from the

boundary layer and escaped through the porous char. In contrast, the reaction of the material during radiant heating is partly due to the transparency of the material to radiation, which produced higher temperatures and pyrolysis reactions in greater depth than did convective heating. These reactions probably occurred at lower temperatures and at different rates to produce different compounds than those resulting from convective heating. However, the reactions in depth occur in a deficiency of oxygen, so that carbon and hydrocarbon products are not oxidized but form the dark layers shown in figure 24. In addition, surface irregularities such as the eroded striations form radiation paths which increase the radiation penetration. As a result of the radiant heating, the material affected by the heating was as great as 60 percent, as compared with 33 percent for test panel 1, which was tested at more severe aerothermal conditions.

The results of testing panel 2 show that radiant heating does not simulate convective heating such as that encountered in flight because of the different temperature gradients produced in the material as a result of different heating and shielding mechanisms in the material. Moreover, during radiant heating there are no aerodynamic shear stresses to remove material from the surface.

CONCLUDING REMARKS

An ablative material (SLA-220) composed of silica-filled elastomeric silicone was tested to evaluate its thermal and structural performance as a heat shield for a hypersonic research aircraft. The SLA-220 was also tested to determine whether it would form a durable char layer when initially heated and thereafter function primarily as an insulator with little further pyrolysis or char removal. Three panels, consisting of the SLA-220 bonded to aluminum substrate panels, were aerothermally tested in the Langley 8-foot high-temperature structures tunnel at heating conditions representative of nominal Mach 6 cruise of the aircraft. Additional tests representative of Mach 8 cruise and interference heating conditions were performed. Radiant heating tests were used to simulate on one panel the complete nominal Mach 6 flight surface-temperature history, which could not be simulated in the tunnel because of run-time limitations.

The structural performance of the SLA-220 during aerothermal tests was poorer than expected. The SLA-220 formed a silica char, but the char was not stable; that is, it did not remain intact after repeated aerothermal exposures at the nominal Mach 6 cruise condition. Both striated and reinforced SLA-220 experienced a general surface recession, with the primary mechanism for char removal being erosion. The erosion was probably due to impacting silica particles which were dislodged from upstream char surfaces by the multidirectional shear forces of the turbulent boundary layer. These particles then impacted the downstream surfaces as a result of the forces of the compressible boundary layer and became increasingly abrasive to the test panel as panel length increased. The streamwise striations increased in width with panel length, and the streamwise edges of the striations became rounded. The reinforced SLA-220 was more resistant to erosion, but shallow streamwise channels formed between the honeycomb cell-wall intersections. The radiant heating tests of the panel, which represented the surface-temperature history of the entire Mach 6 flight,

showed that radiant heating is not a valid technique for simulating aerodynamic heating of the SLA-220 material. The different heat-transfer mechanisms of radiant heating caused more severe degradation of the SLA-220 than that of aerothermal heating.

Langley Research Center
National Aeronautics and Space Administration
Hampton, VA 23665
September 23, 1977

REFERENCES

1. Kirkham, F. S.; Jones, R. A.; Buck, M. L.; and Zima, W. P.: Joint USAF/NASA Hypersonic Research Aircraft Study. AIAA Paper No. 75-1039, Aug. 1975.

2. Brackeen, Richard E.; and Marcy, William L.: X-24B Growth Version Feasibility Study. AFFDL-TR-73-116, U.S. Air Force, Oct. 1973. (Available from DDC as AD 917 976L.)

3. Plank, P. Paul; Marcy, William L.; and Haefeli, Rudolph C.: Experiments Impact on X-24C. AFFDL-TR-75-37, U.S. Air Force, May 1975. (Available from DDC as AD B005 003L.)

4. Metric Practice Guide. E 380-72, American Soc. Testing & Mater., June 1972.

5. Deveikis, William D.; and Hunt, L. Roane: Loading and Heating of a Large Flat Plate at Mach 7 in the Langley 8-Foot High-Temperature Structures Tunnel. NASA TN D-7275, 1973.

6. Ames Research Staff: Equations, Tables, and Charts for Compressible Flow. NACA Rep. 1135, 1953. (Supersedes NACA TN 1428.)

7. Deveikis, William D.; Bruce, Walter E., Jr.; and Karns, John R.: Techniques for Aerothermal Tests of Large, Flightweight Thermal Protection Panels in a Mach 7 Wind Tunnel. AIAA Paper No. 74-617, July 1974.

8. Kendall, Robert M.: An Analysis of the Coupled Chemically Reacting Boundary Layer and Charring Ablator. Part V - A General Approach to the Thermochemical Solution of Mixed Equilibrium-Nonequilibrium, Homogeneous or Heterogeneous Systems. NASA CR-1064, 1968.

9. Anderson, E. C.; and Lewis, C. H.: Laminar or Turbulent Boundary-Layer Flows of Perfect Gases or Reacting Gas Mixtures in Chemical Equilibrium. NASA CR-1893, 1971.

TABLE I.- AEROTHERMAL CRUISE CONDITIONS FOR A HYPERSONIC RESEARCH AIRCRAFT

(a) Free-stream conditions

	Mach 6[a]	Mach 7	Mach 8
Altitude, km (ft)	26.8 (88 000)	28.8 (94 600)	30.8 (101 000)
Dynamic pressure, kPa (lb/ft^2)	48.65 (1016)	48.89 (1021)	47.69 (996)
Angle of attack, deg	5 to 5.7	5	5
Total enthalpy, kJ/kg (Btu/lb)	1860 (800)	2240 (964)	2954 (1271)

(b) Condition at reference location[b]

[Turbulent boundary layer]

	Mach 6[a]	Mach 7	Mach 8
Reynolds number	12.5 x 10^6	11.2 x 10^6	9.9 x 10^6
Heat flux (cold wall), kW/m^2 (Btu/ft^2-sec)	136 to 159 (12 to 14)	148 to 182 (13 to 16)	193 to 227 (17 to 20)
Shear stress (hot wall), Pa (lb/ft^2)	134 to 148 (2.8 to 3.1)	134 to 148 (2.8 to 3.1)	134 to 148 (2.8 to 3.1)
Surface temperature:			
Maximum, K ($^\circ$R)	1033 (1860)	1183 (2130)	1283 (2310)
Minimum, K ($^\circ$R)	964 (1735)	992 (1785)	1033 (1860)

[a]Nominal Mach 6 cruise condition. (See fig. 1.)
[b]254 cm (100 in.) from nose.

TABLE II.- MOLE FRACTIONS OF TEST-MEDIUM CONSTITUENTS

(a) Test panel 1

Test	Mole fraction of -				
	O_2	N_2	CO_2	H_2O	Ar
1	0.116	0.745	0.043	0.085	0.0089
2	.104	.743	.048	.095	.0088
3	.087	.737	.056	.111	.0088
4	.081	.735	.058	.117	.0088
5	.081	.735	.058	.117	.0088
6	.087	.737	.056	.111	.0088
7	.104	.744	.048	.095	.0088
8	.056	.727	.069	.139	.0086
9	.107	.745	.046	.093	.0089
10	.096	.741	.051	.103	.0088
11	.050	.724	.072	.145	.0086
12	.065	.730	.065	.131	.0087

(b) Test panel 2

Test	Mole fraction of -				
	O_2	N_2	CO_2	H_2O	Ar
1	0.0747	0.733	0.0611	0.122	0.0087
2	↓	↓	↓	↓	↓
3	↓	↓	↓	↓	↓
4	↓	↓	↓	↓	↓
5	.0436	.722	.0752	.150	.0086
6	↓	↓	↓	↓	↓
7	↓	↓	↓	↓	↓
8	↓	↓	↓	↓	↓
9	↓	↓	↓	↓	↓

(c) Test panel 3

Test	Mole fraction of -				
	O_2	N_2	CO_2	H_2O	Ar
1	0.0436	0.722	0.0752	0.150	0.0086
2	↓	↓	↓	↓	↓
3	↓	↓	↓	↓	↓
4	↓	↓	↓	↓	↓
5	↓	↓	↓	↓	↓
6	↓	↓	↓	↓	↓
7	.096	.741	.051	.103	.0088

TABLE III.- TEST CONDITIONS

(a) Test panel 1

Test	Combustor total pressure		Total temperature		Free-stream pressure		Free-stream dynamic pressure	
	MPa	lb/in^2	K	^{o}R	kPa	lb/in^2	kPa	lb/ft^2
1	17.0	2470	1278	2300	2.10	0.305	54.9	1150
2	6.81	987	1389	2500	.855	.124	20.5	429
3	6.81	987	1556	2800	.917	.133	23.7	495
4	17.1	2490	1611	2900	2.39	.347	62.7	1310
5	17.1	2480	1611	2900	2.19	.317	58.8	1230
6	17.0	2470	1556	2800	2.11	.306	54.3	1130
[a]7	6.76	980	1389	2500	.862	.125	27.8	581
[a]8	6.76	980	1833	3300	.813	.118	25.5	533
9	17.0	2470	1361	2450	2.15	.312	70.1	1470
10	16.9	2450	1472	2650	2.32	.337	75.8	1580
11	17.2	2500	1889	3400	2.12	.308	68.9	1440
12	17.1	2480	1750	3150	1.99	.288	66.8	1400

Test	Test duration, s	Angle of attack, deg	Total enthalpy		Local Reynolds number		Local Mach number	Heat flux (cold wall)		Shear stress (hot wall)	
			kJ/kg	Btu/lb	per m	per ft		kW/m^2	Btu/ft^2-sec	Pa	lb/ft^2
1	63	0	1480	635	8.14×10^6	1.87×10^6	5.93	45.4	4.0	57.5	1.20
2	51	0	1620	695	2.60	.791	5.75	25.0	2.2	29.2	.61
3	47	0	1860	800	2.46	.748	6.00	31.8	2.8	34.0	.71
4	27	0	1940	835	5.58	1.70	6.21	63.6	5.6	66.1	1.38
5	54	0	1940	835	5.48	1.67	6.23	64.7	5.7	63.7	1.33
6	76	0	1860	800	5.29	1.61	6.08	59.0	5.2	58.9	1.23
[a]7	41	15	1620	695	6.67	2.03	4.82	93.1	8.2	96.7	2.02
[a]8	41	15	2280	980	4.43	1.35	4.51	144	12.7	113	2.36
9	41	15	1590	685	17.1	5.21	4.90	194	17.1	192	4.00
10	32	15	1880	810	15.6	4.76	4.77	218	19.2	200	4.17
11	27	15	2370	1020	11.6	3.53	4.60	306	27.0	231	4.83
12	31	15	2130	915	13.2	4.03	4.60	301	26.5	232	4.85

[a]Nominal Mach 6 cruise conditions.

TABLE III.- Continued

(b) Test panel 2

Test	Combustor total pressure		Total temperature		Free-stream pressure		Free-stream dynamic pressure	
	MPa	lb/in^2	K	^{o}R	kPa	lb/in^2	kPa	lb/ft^2
1	17.2	2500	1670	3000	1.99	0.288	63.2	1320
2	17.2	2490	1670	3000	1.94	.281	61.2	1280
3	17.2	2500	1670	3000	2.03	.295	64.4	1340
4	17.2	2490	1670	3000	2.04	.296	61.9	1290
5	17.2	2490	1940	3500	1.97	.286	68.7	1440
6	17.2	2490	1940	3500	1.94	.282	67.6	1410
7	17.4	2520	1940	3500	2.08	.302	70.6	1470
8	17.2	2490	1940	3500	1.91	.277	66.1	1380
9	17.2	2500	1940	3500	1.90	.275	63.3	1320

Test	Test duration, s	Angle of attack, deg	Total enthalpy		Local Reynolds number		Local Mach number	Heat flux (cold wall)		Shear stress (hot wall)	
			kJ/kg	Btu/lb	per m	per ft		kW/m^2	Btu/ft^2-sec	Pa	lb/ft^2
1	41	7	2040	875	10.7 $\times 10^6$	3.26 $\times 10^6$	5.90	143	12.6	128	2.68
2	41	7	↓	↓	10.9	3.31	5.71	144	12.7	131	2.73
3	40	7	↓	↓	10.5	3.19	5.71	129	11.4	130	2.72
4	41	7	↓	↓	10.1	3.07	5.61	129	11.4	122	2.54
5	41	7	2470	1060	9.25	2.82	5.94	157	13.8	132	2.76
6	41	7	↓	↓	9.48	2.89	5.95	163	14.4	135	2.82
7	41	7	↓	↓	9.61	2.93	5.93	163	14.4	137	2.86
8	41	7	↓	↓	9.48	2.89	5.93	163	14.4	135	2.82
9	41	7	↓	↓	9.58	2.92	5.93	157	13.8	133	2.78

TABLE III.- Concluded

(c) Test panel 3

Test	Combustor total pressure		Total temperature		Free-stream pressure		Free-stream dynamic pressure	
	MPa	lb/in^2	K	^{o}R	kPa	lb/in^2	kPa	lb/ft^2
1	17.0	2460	1940	3500	1.92	0.279	66.7	1390
2	17.0	2460	1940	3500	1.92	.279	66.7	1390
3	17.0	2460	1940	3500	1.92	.279	66.7	1390
4	17.0	2460	1940	3500	1.92	.279	66.7	1390
5	17.0	2470	1940	3500	1.93	.280	67.0	1400
6	17.0	2460	1940	3500	1.92	.279	66.7	1390
7	17.3	2510	1500	2700	2.38	.345	77.6	1620

Test	Test duration, s	Angle of attack, deg	Total enthalpy		Local Reynolds number		Local Mach number	Heat flux (cold wall)		Shear stress (hot wall)	
			kJ/kg	Btu/lb	per m	per ft		kW/m^2	Btu/ft^2-sec	Pa	lb/ft^2
1	40	7	2470	1060	9.61×10^6	2.93×10^6	5.93	163	14.4	137	2.86
2	40	↓	↓	↓	↓	↓	↓	↓	↓	↓	↓
3	40	↓	↓	↓	↓	↓	↓	↓	↓	↓	↓
4	11	↓	↓	↓	↓	↓	↓	↓	↓	↓	↓
5	59	↓	↓	↓	↓	↓	↓	↓	↓	↓	↓
6	65	↓	↓	↓	↓	↓	↓	↓	↓	↓	↓
7	15	15	1920	825	15.6	4.76	4.80	227	20.0	202	4.20

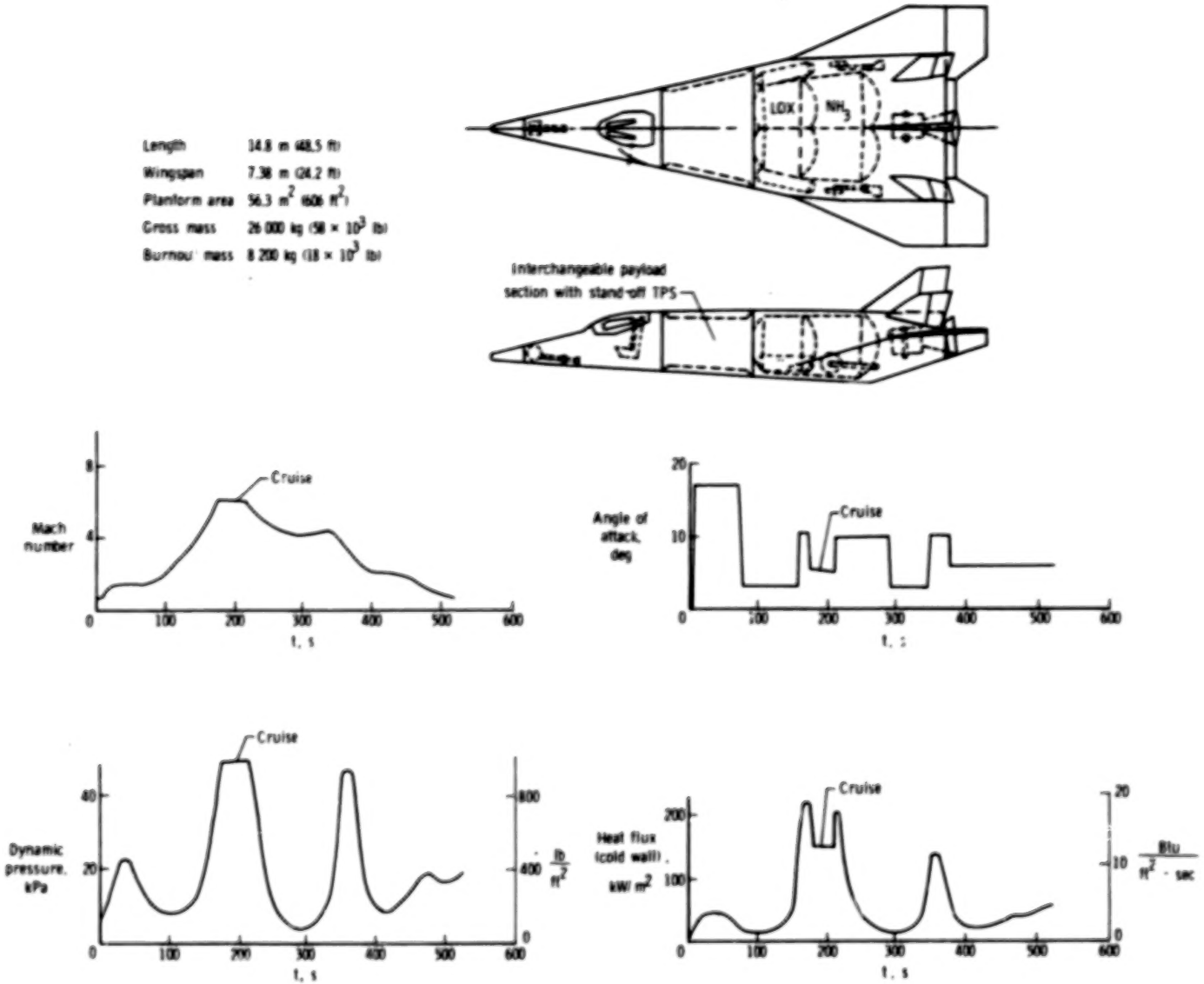

Figure 1.- Hypersonic research aircraft and nominal Mach 6 trajectory.
(Reference location for heat flux: 254 cm (100 in.) from nose.)

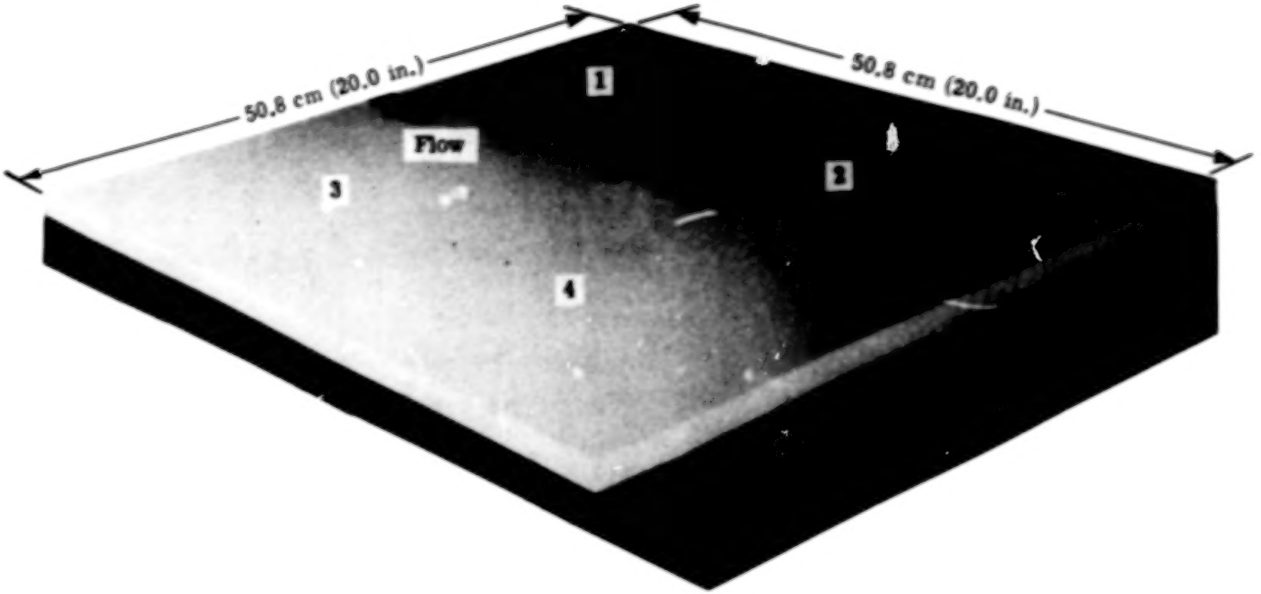

L-75-831.1

Figure 2.- Test panel 1 before testing.

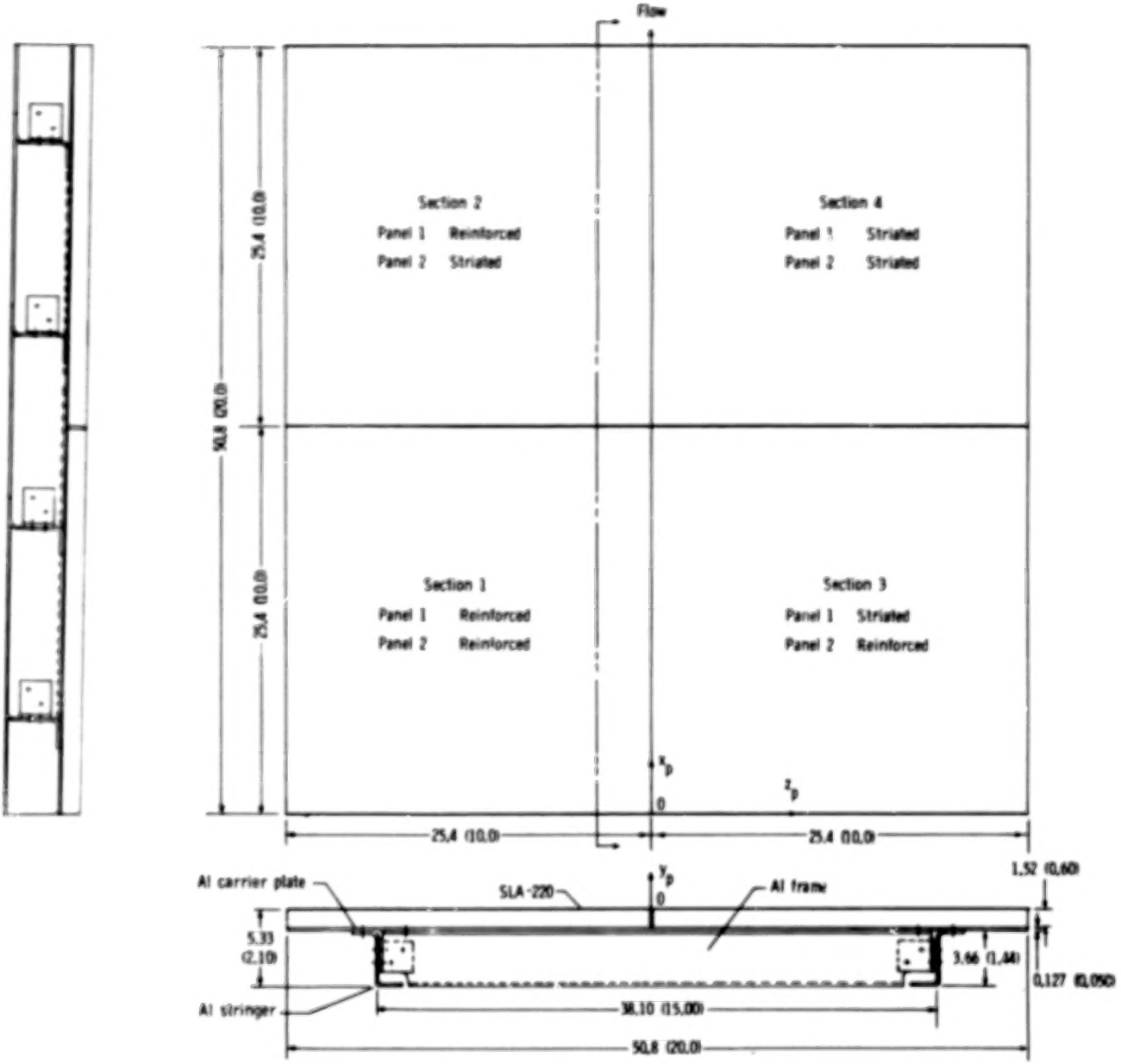

(a) Panels 1 and 2.

Figure 3.- Test panels. All dimensions are in cm (in.).

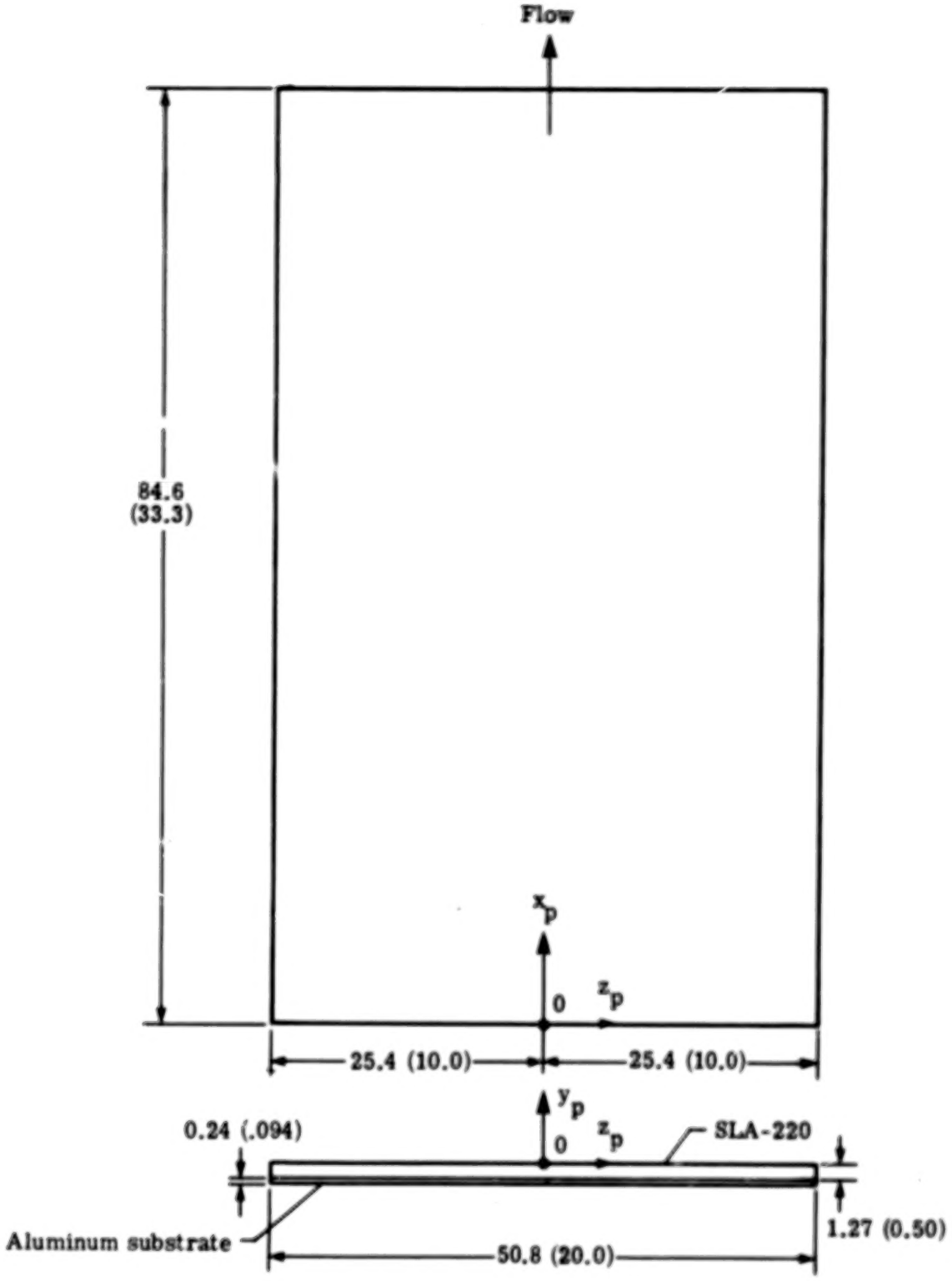

(b) Panel 3 (striated).

Figure 3.- Concluded.

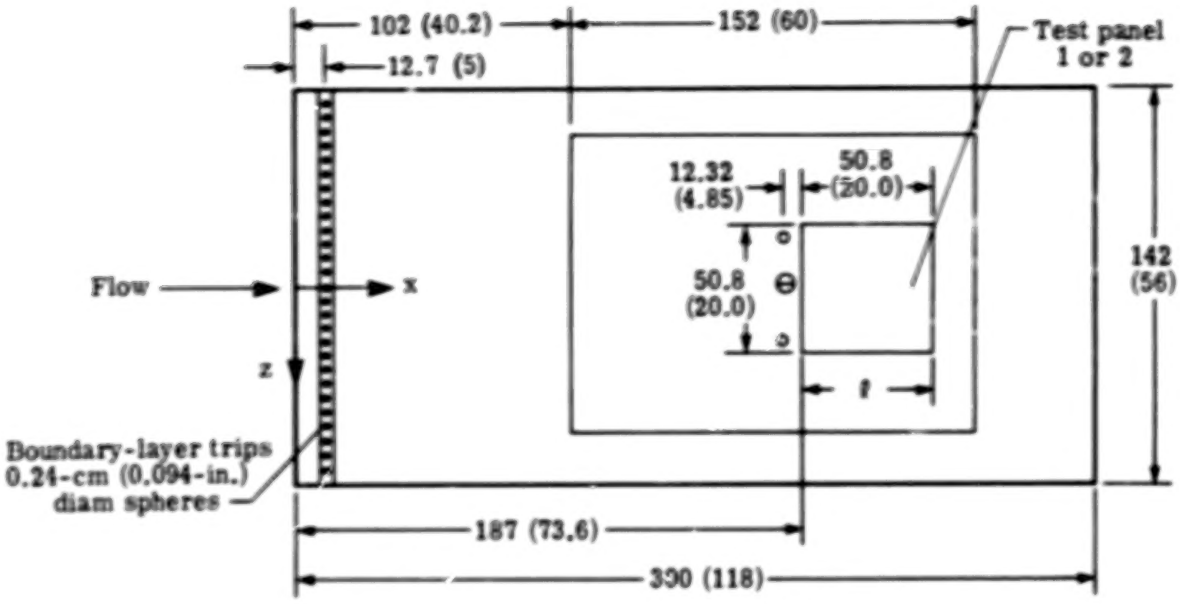

(a) Test panel 1 or 2 installed.

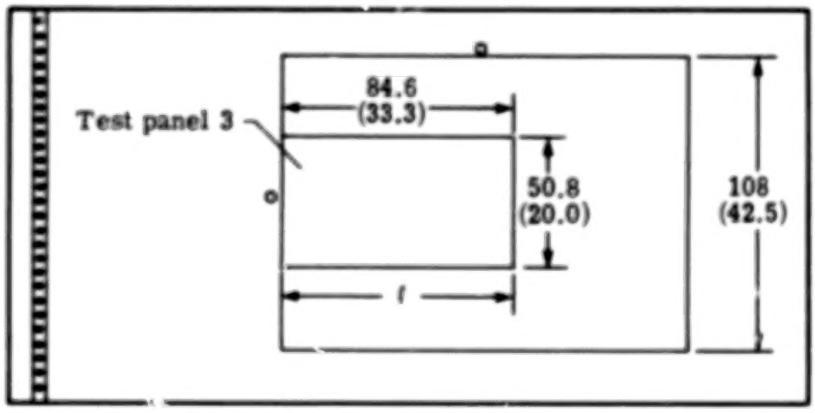

(b) Test panel 3 installed.

∘ Surface pressure orifice

⊖ Boundary-layer probe

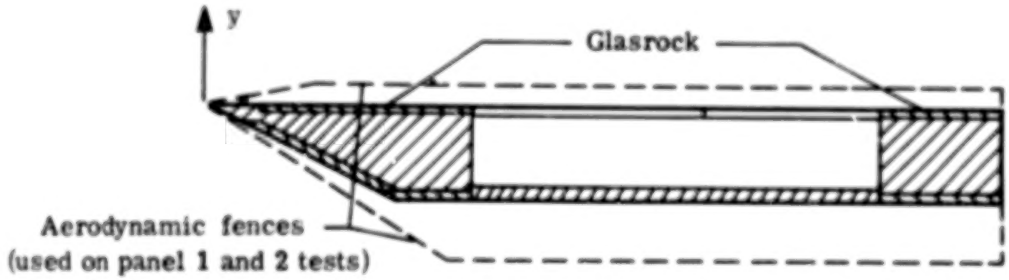

(c) Cross section of panel holder (test panel 3 installed).

Figure 4.- Panel holder details and instrumentation.
All dimensions are in cm (in.).

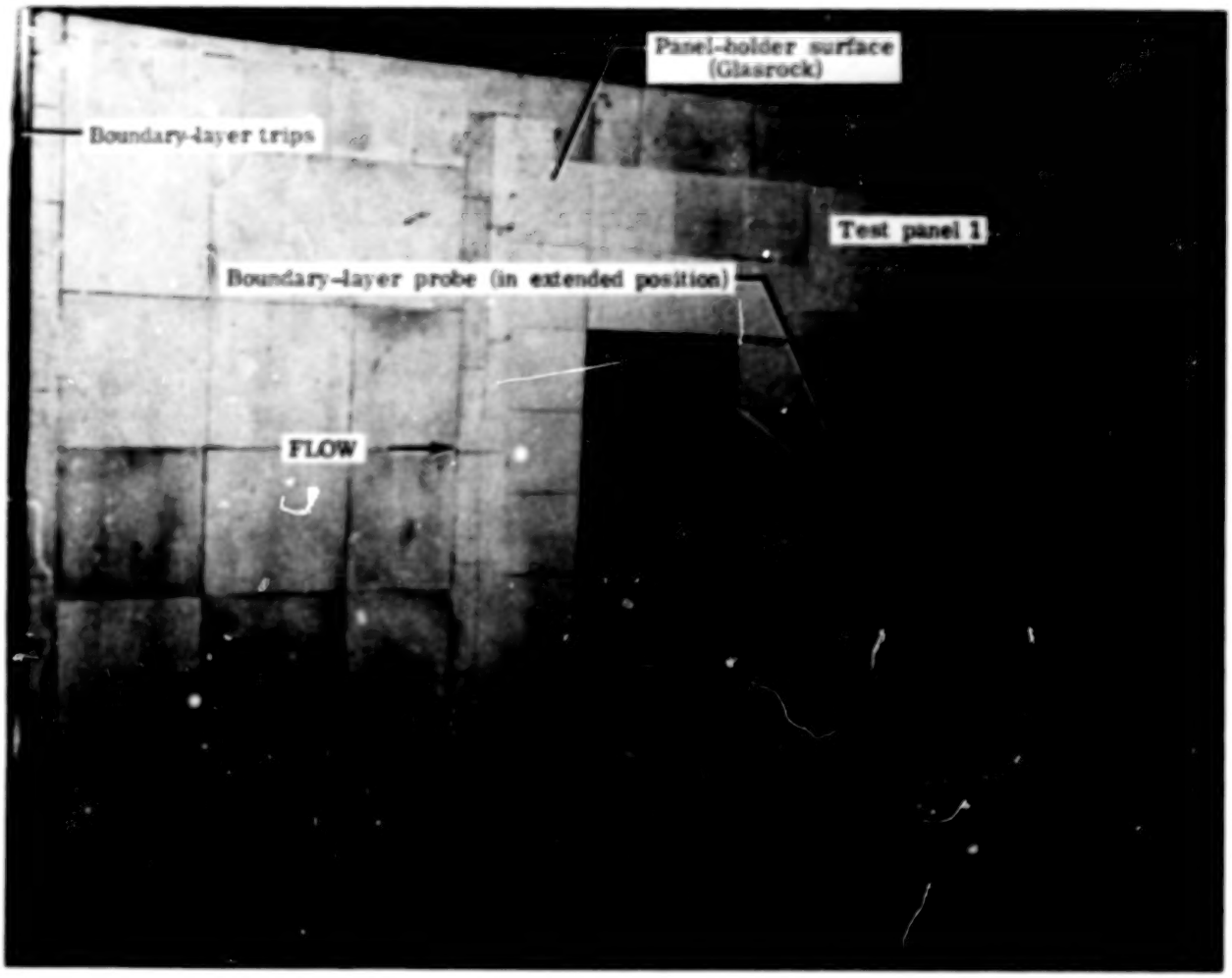

L-75-3291.1

Figure 5.- Top view of panel holder in test section.

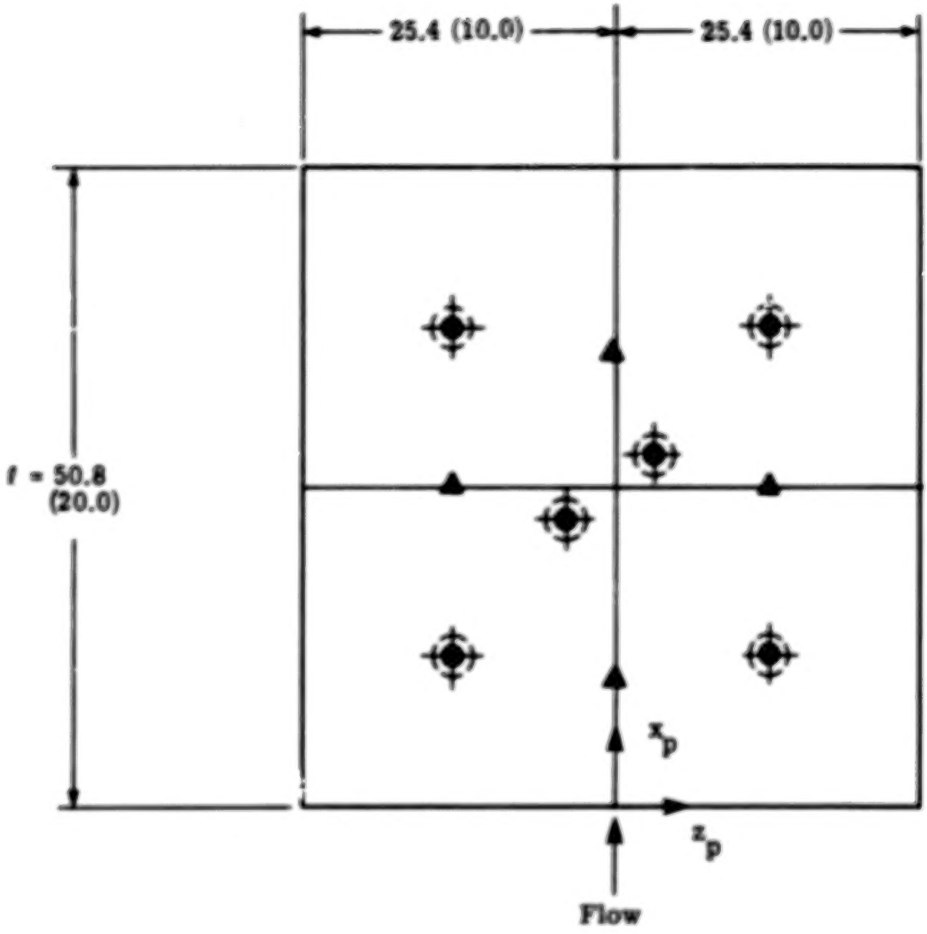

Thermocouple location

x_p/l	z_p/l
Thermocouple in plug and on back surface (●)	
0.238	-0.250
0.238	0.250
0.450	-0.075
0.550	0.075
0.750	-0.250
0.750	0.250
Back surface thermocouples (▲)	
0.200	0
0.500	-0.250
0.500	0.250
0.700	0

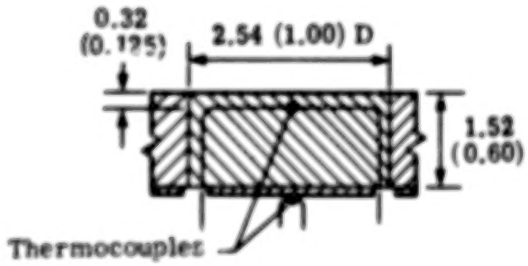

Typical thermocouple installation in plug and on back surface

Figure 6.- Thermocouple locations and installation details for test panels 1 and 2. All dimensions are in cm (in.).

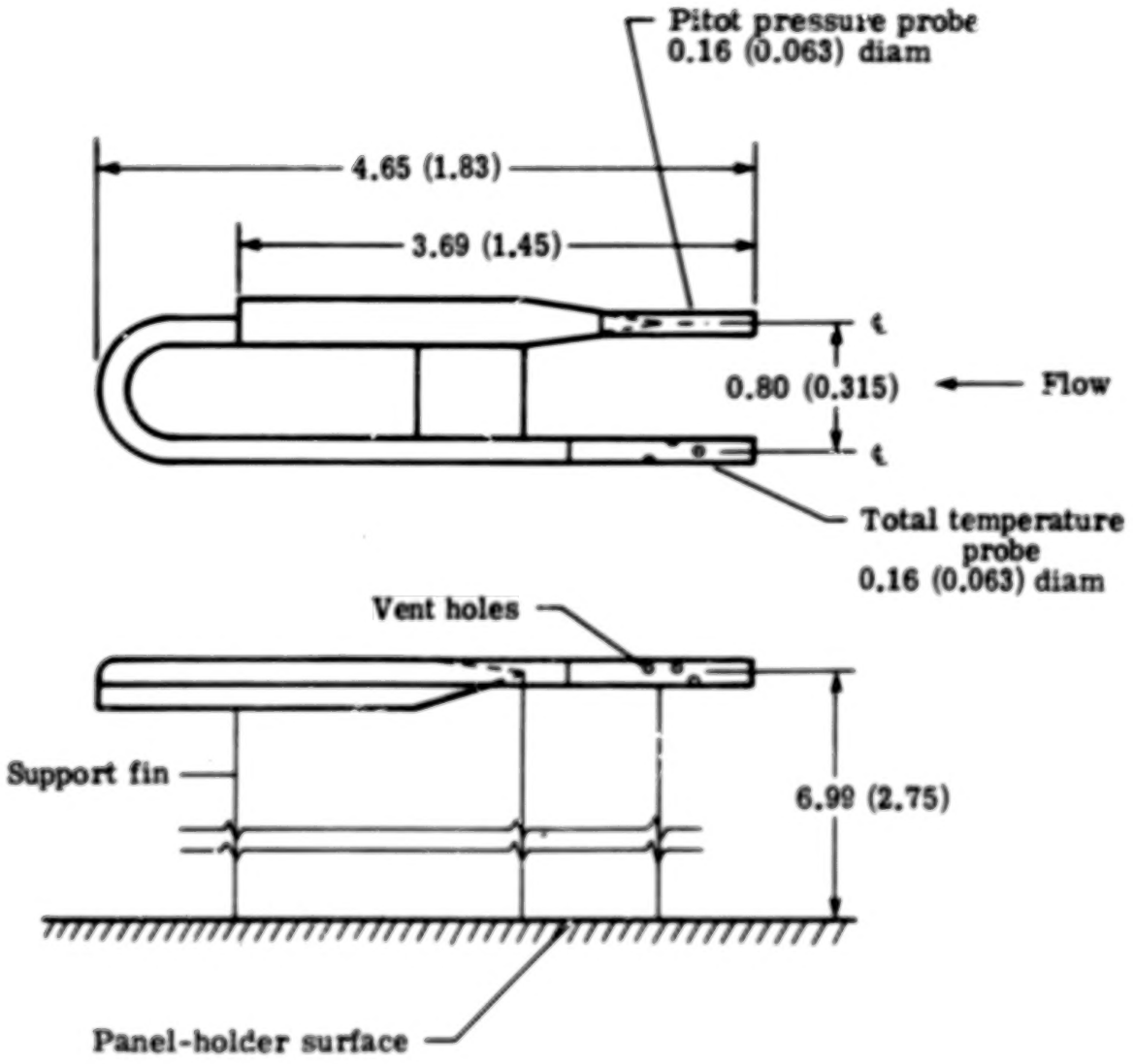

(a) Schematic of probe.

Figure 7.- Boundary-layer survey probe. All dimensions are in cm (in.).

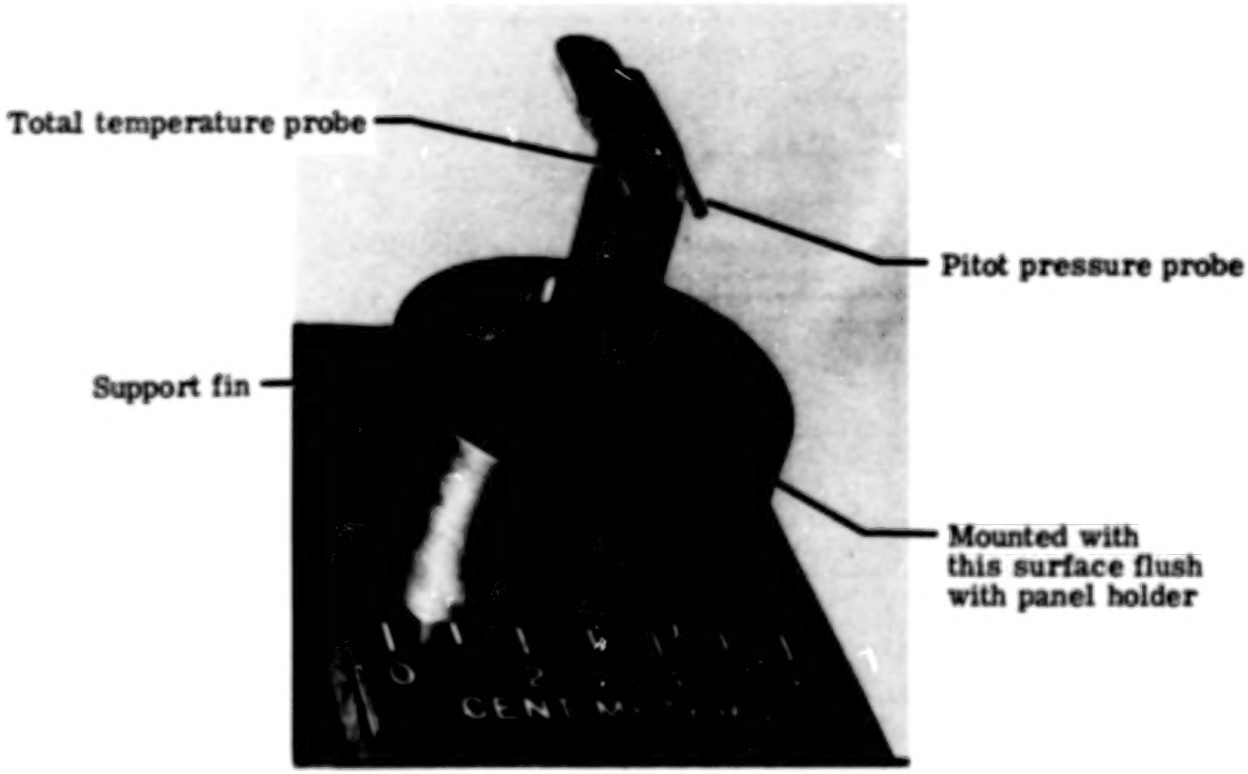

(b) Probe in extended position.

Figure 7.- Concluded.

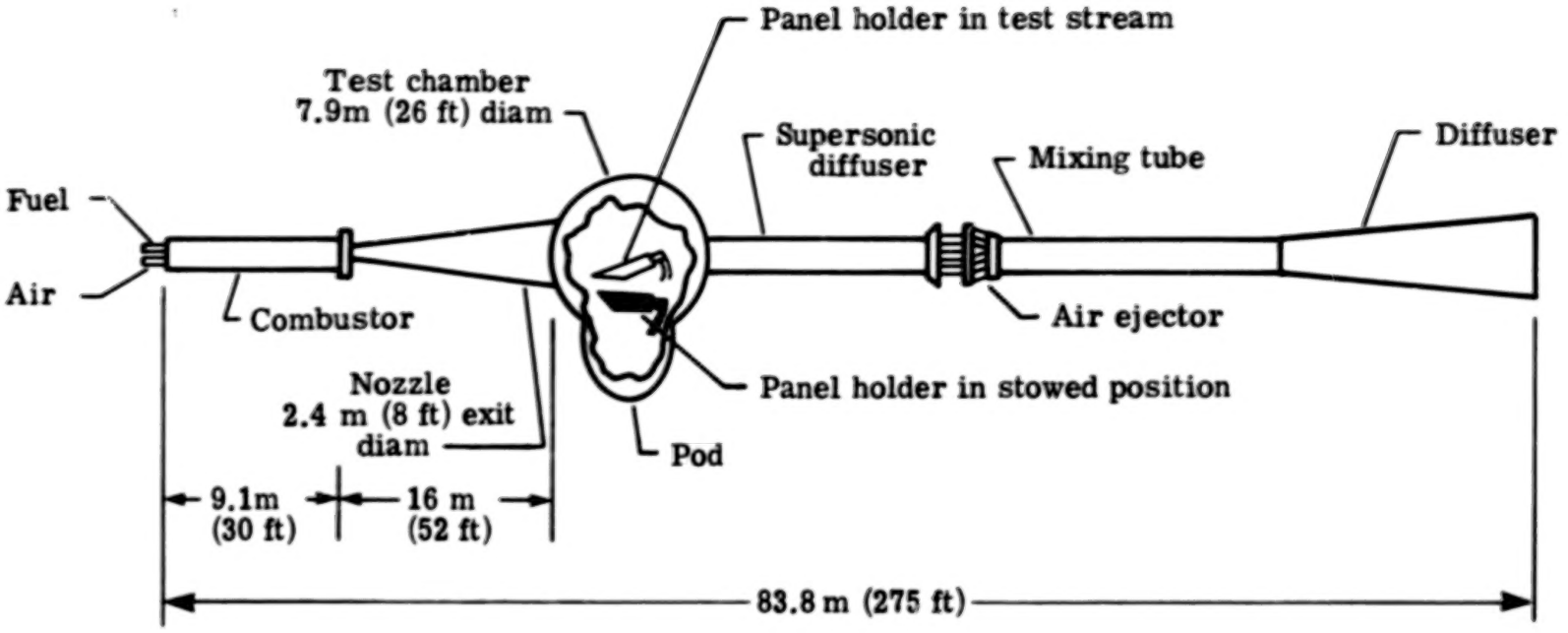

Figure 8.- Langley 8-foot high-temperature structures tunnel.

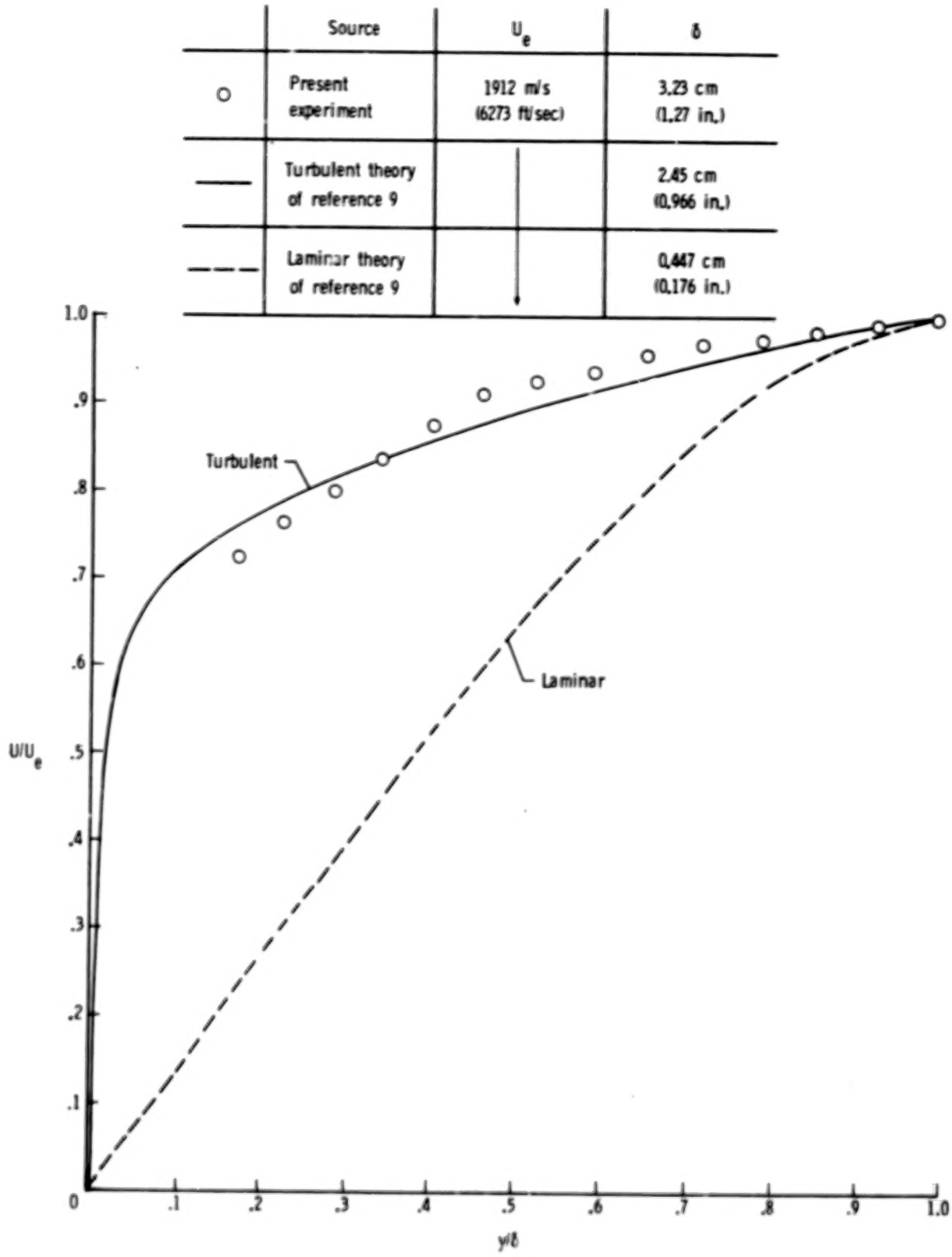

Figure 9.- Boundary-layer velocity profile. Panel-holder angle of attack, 7°; test 7 on test panel 2.

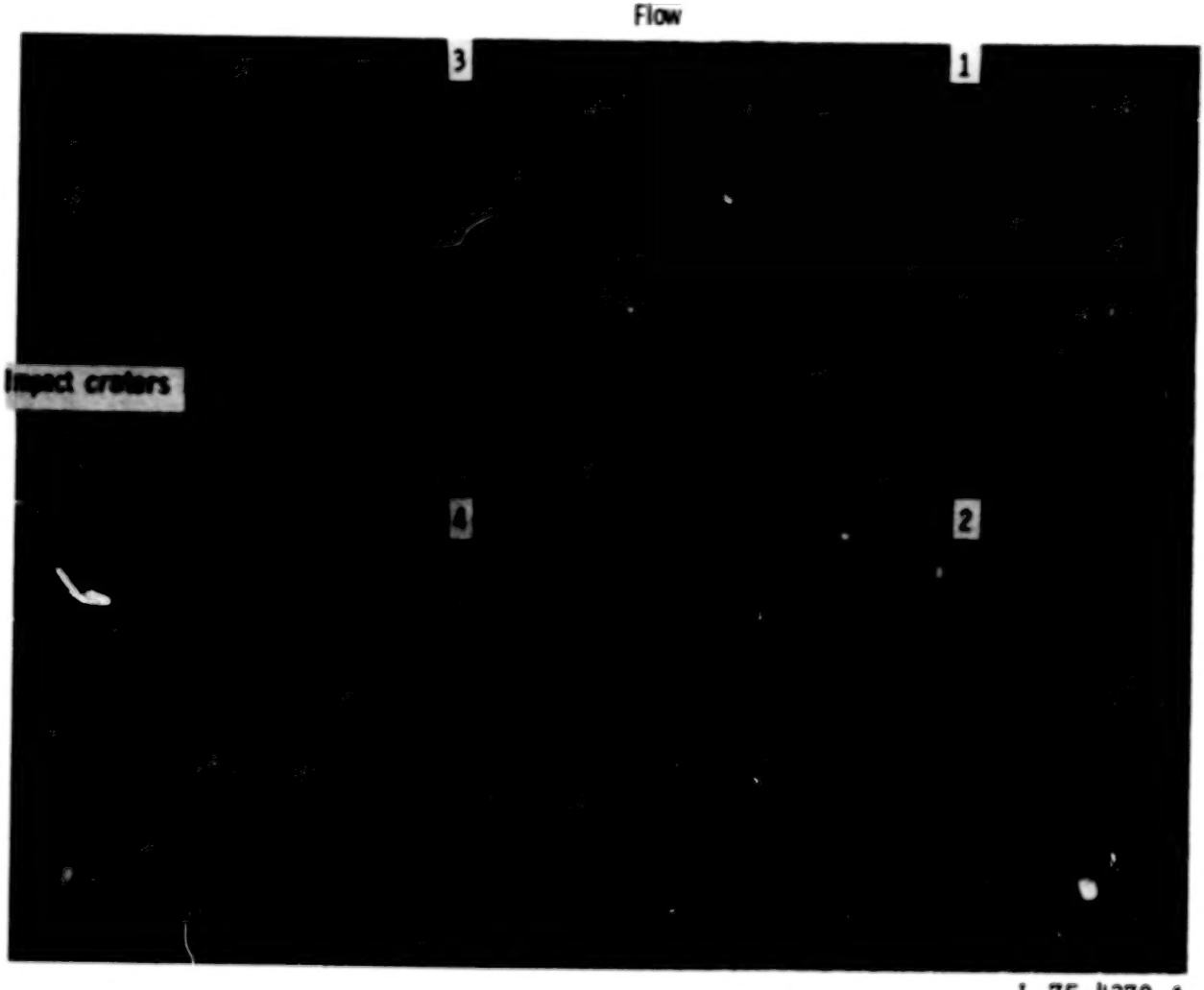

L-75-4370.1

Figure 10.- Panel 1 after test 8.

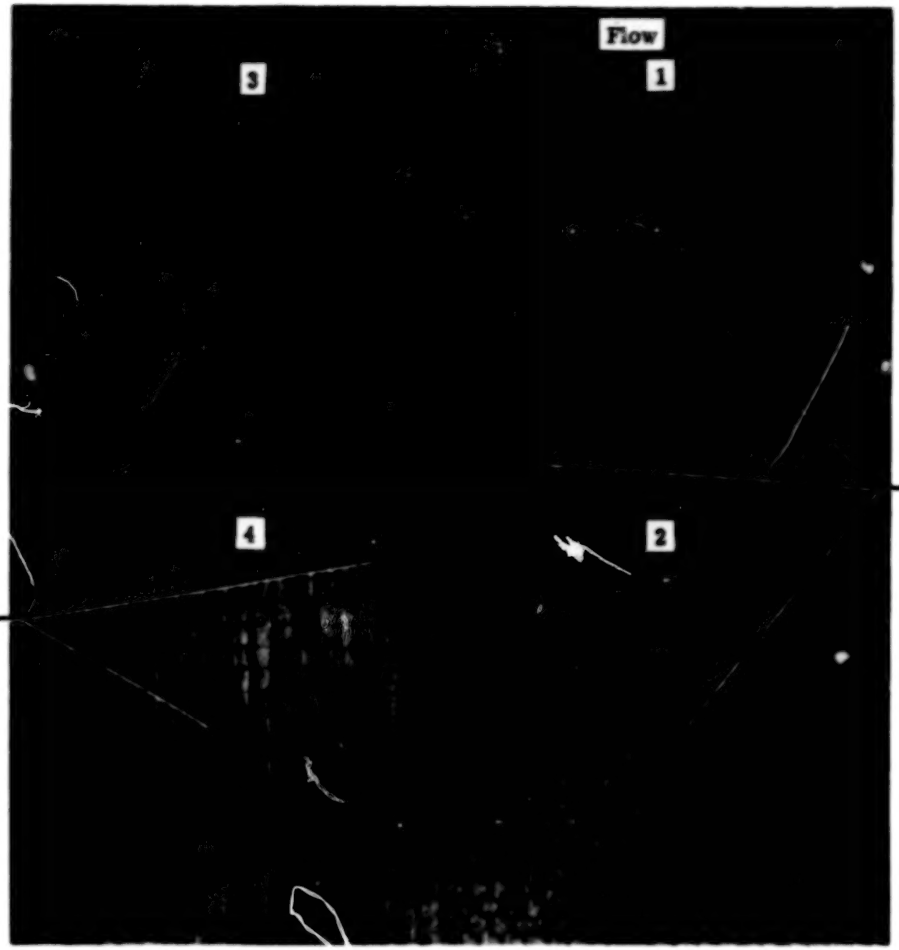

L-75-5013.1

Figure 11.- Panel 1 after test 10.

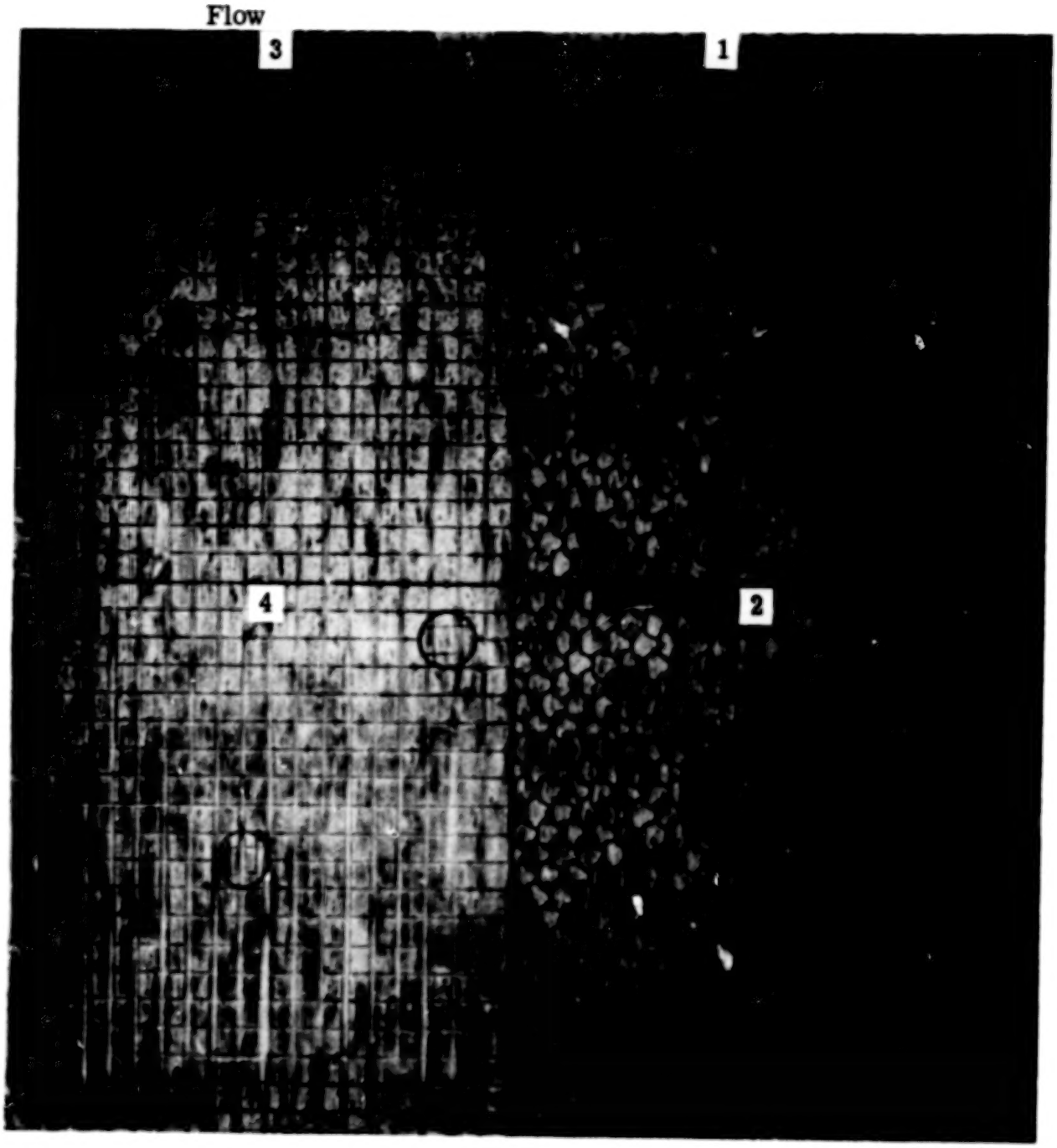

L-75-5264.1

Figure 12.- Panel 1 after test 12.

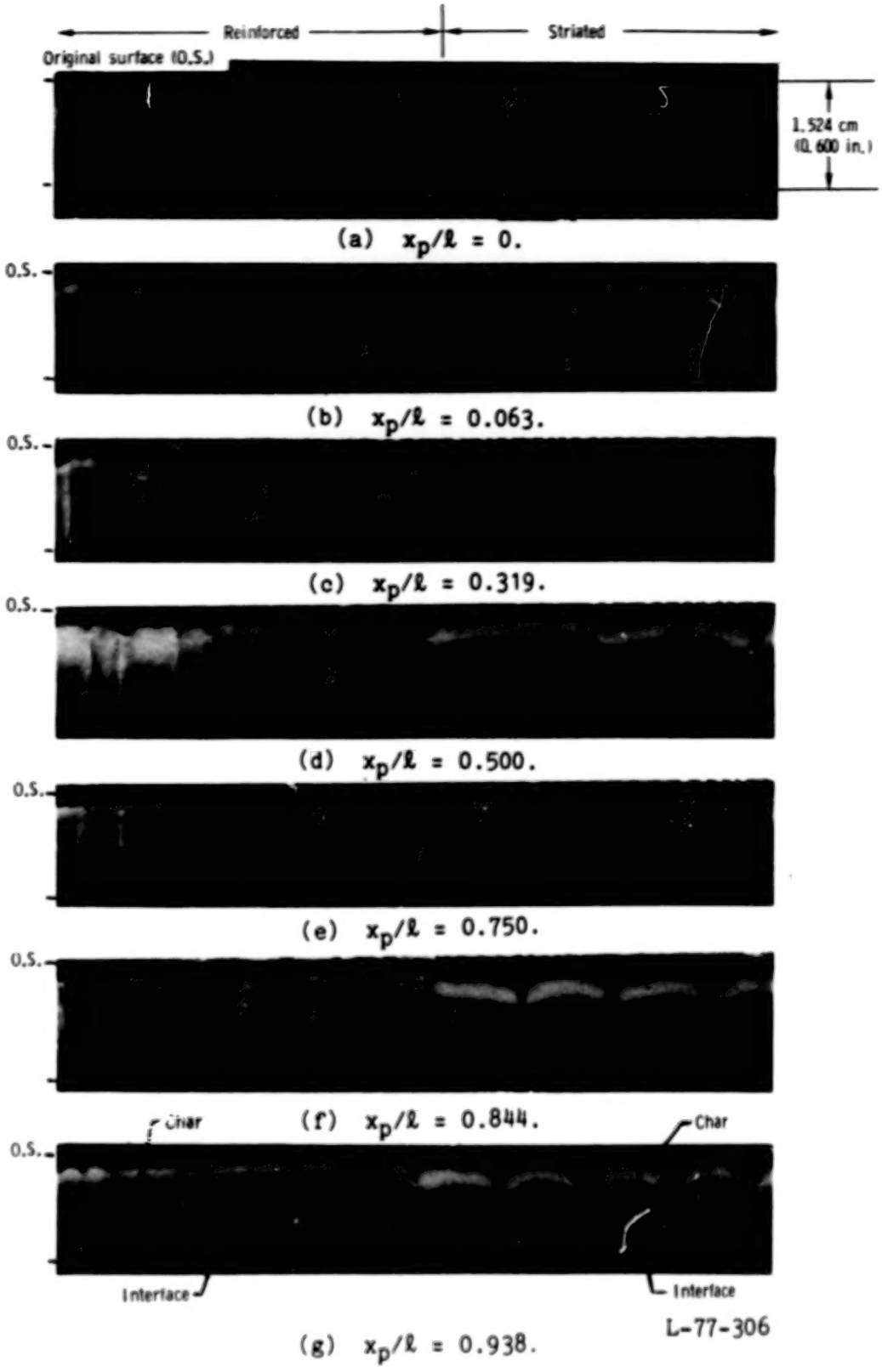

Figure 13.- Spanwise-section photographs of test panel 1.- ℓ = 50.8 cm (20.0 in.).

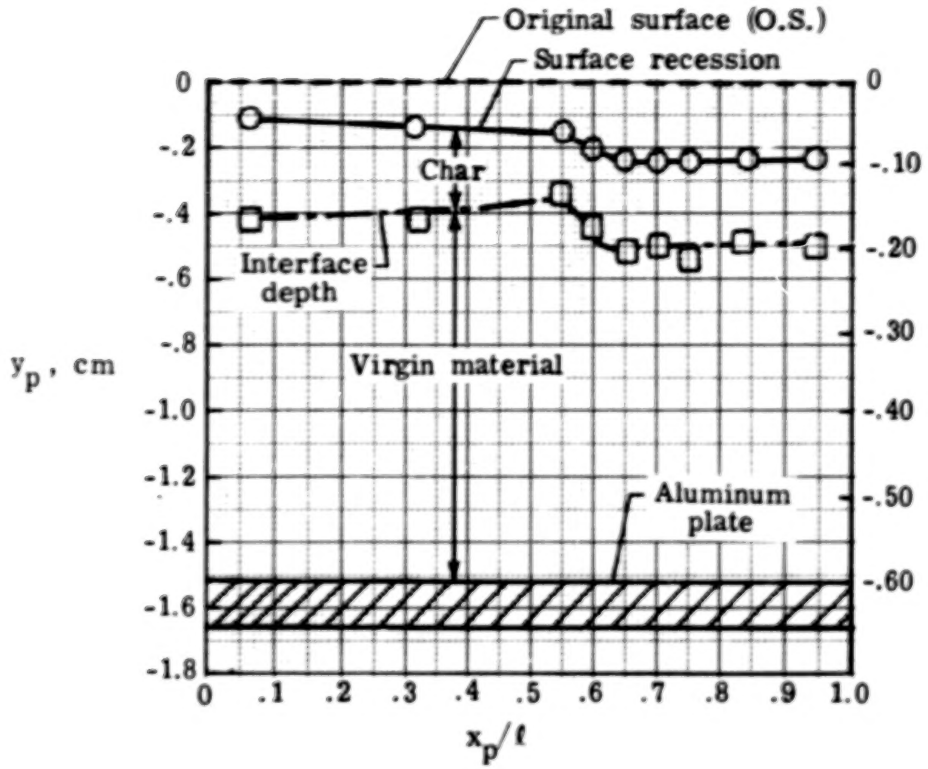

(a) Striated sections.

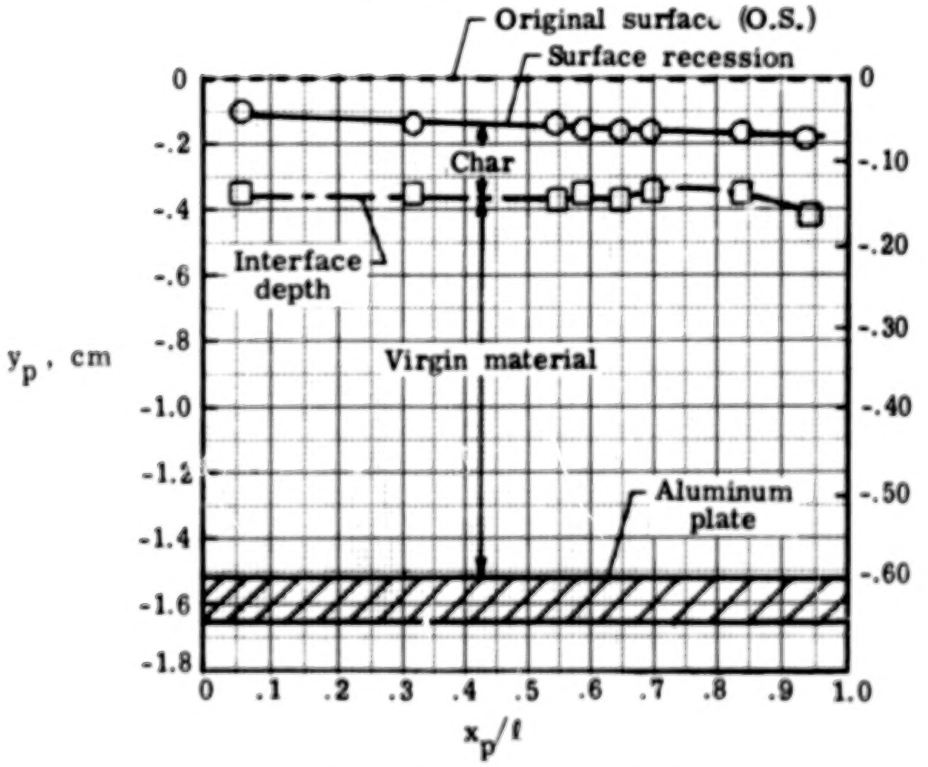

(b) Reinforced sections.

Figure 14.- Distribution of surface recession and char–virgin-material interface depth for panel 1 after test completion.

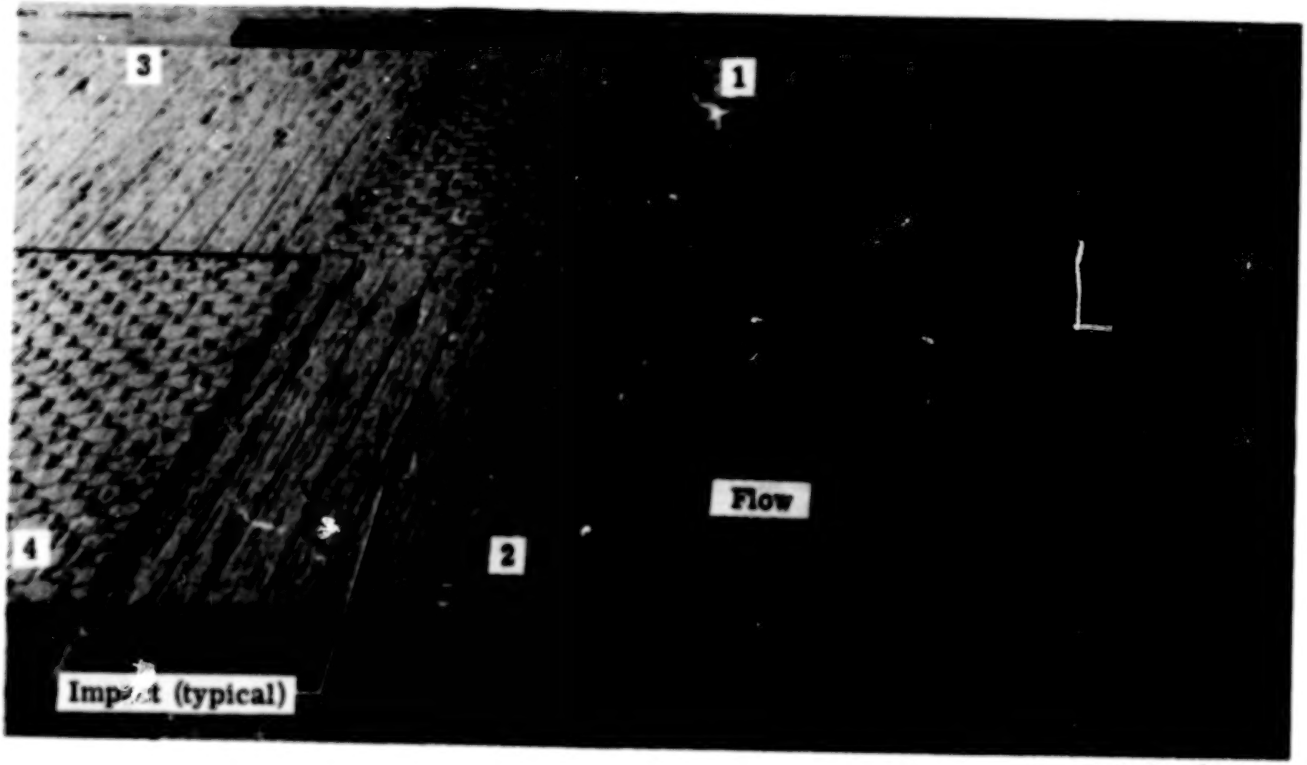

L-75-6503.1

Figure 15.- Panel 2 after test 3.

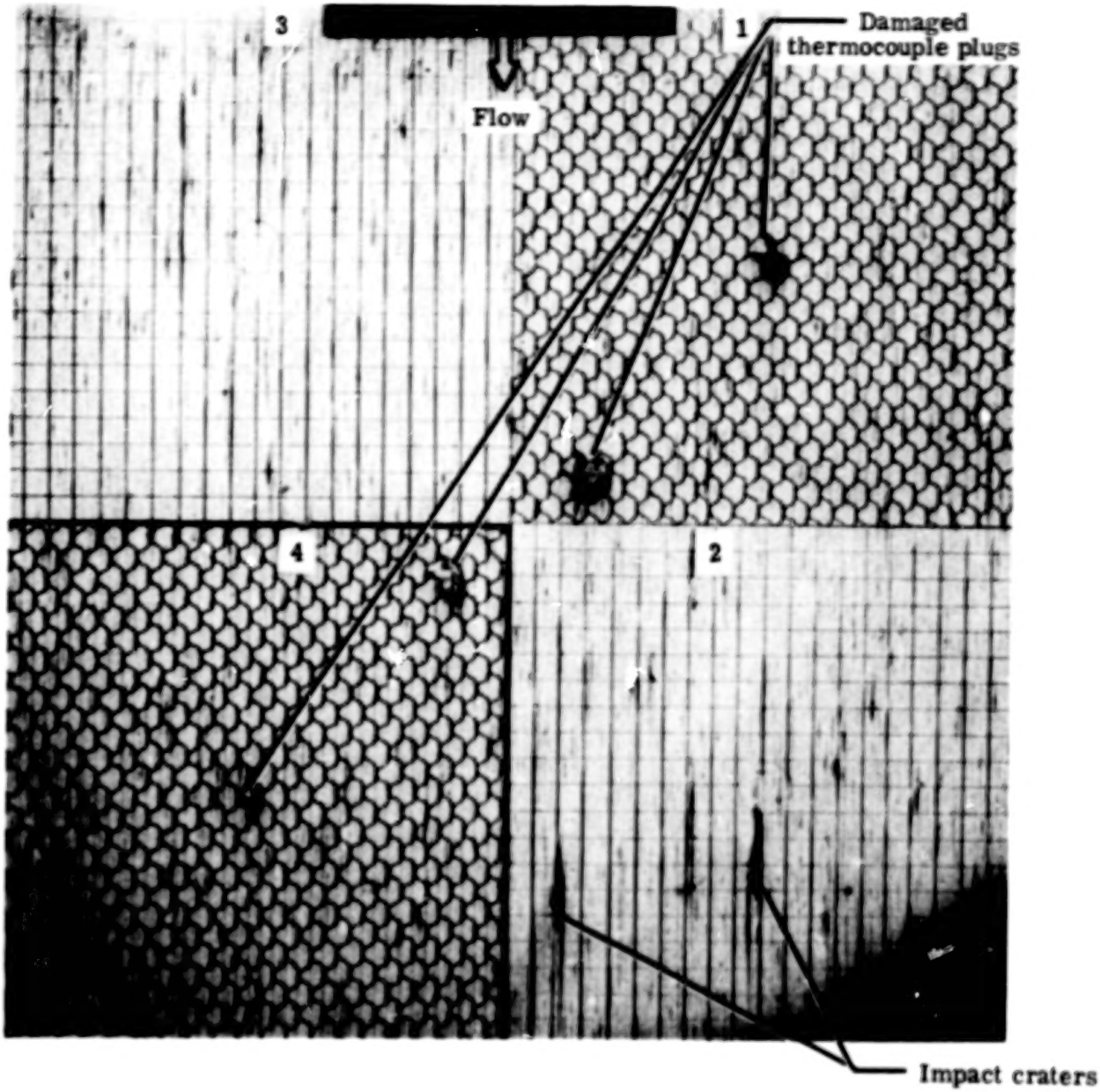

(a) Overall view.

L-75-7006.1

Figure 16.- Panel 2 after test 9.

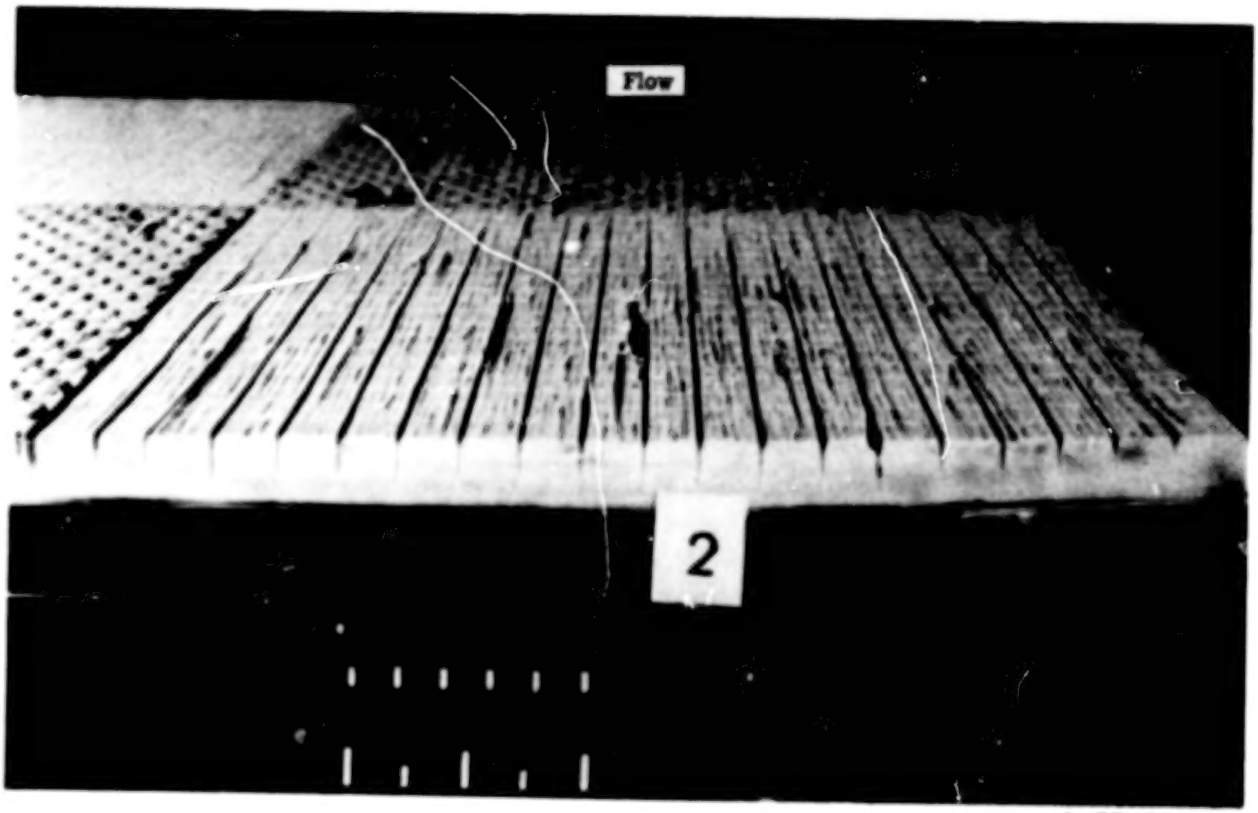

L-75-7031.1

(b) Striated section.

Figure 16.- Continued.

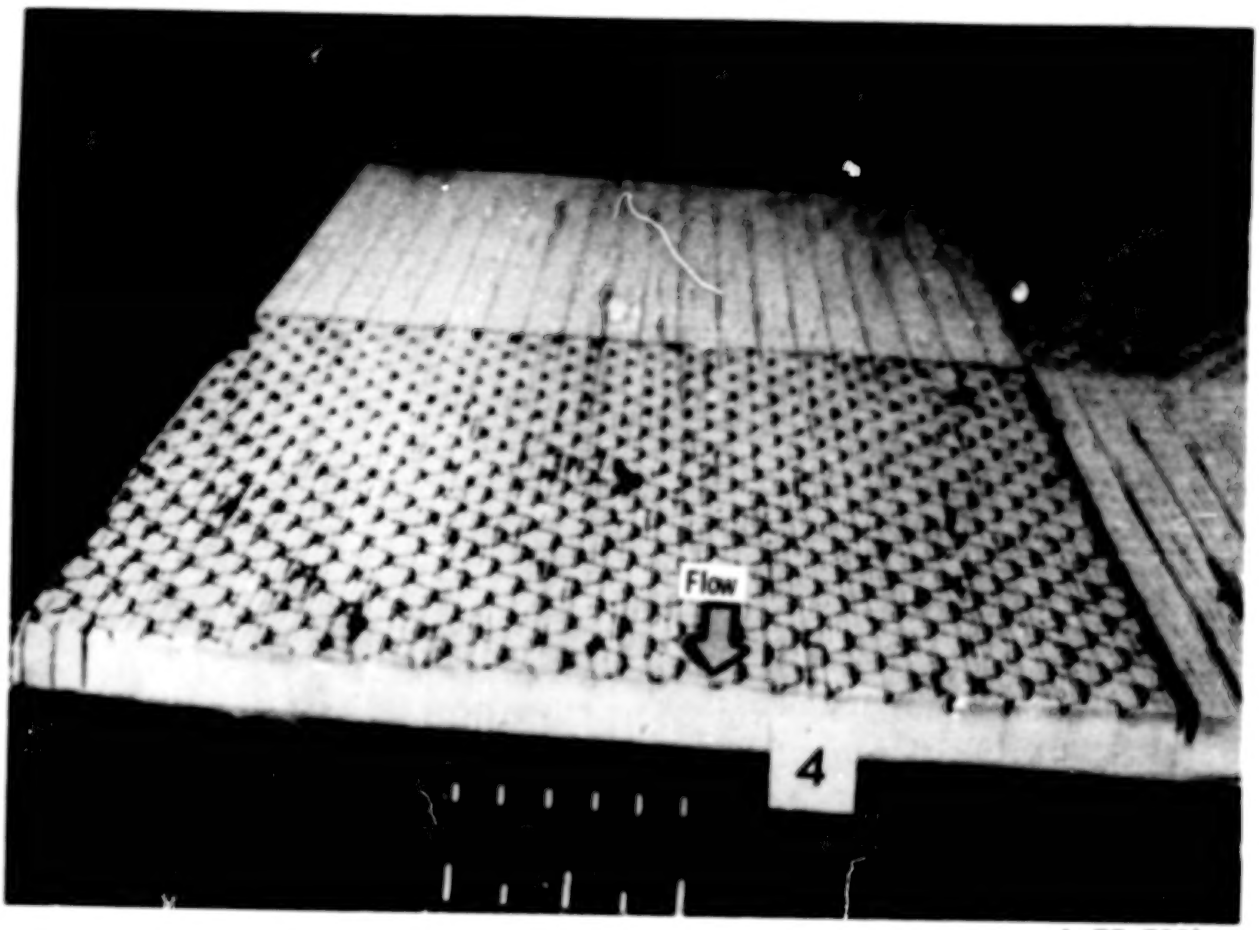

L-75-7024.1

(c) Reinforced section.

Figure 16.- Concluded.

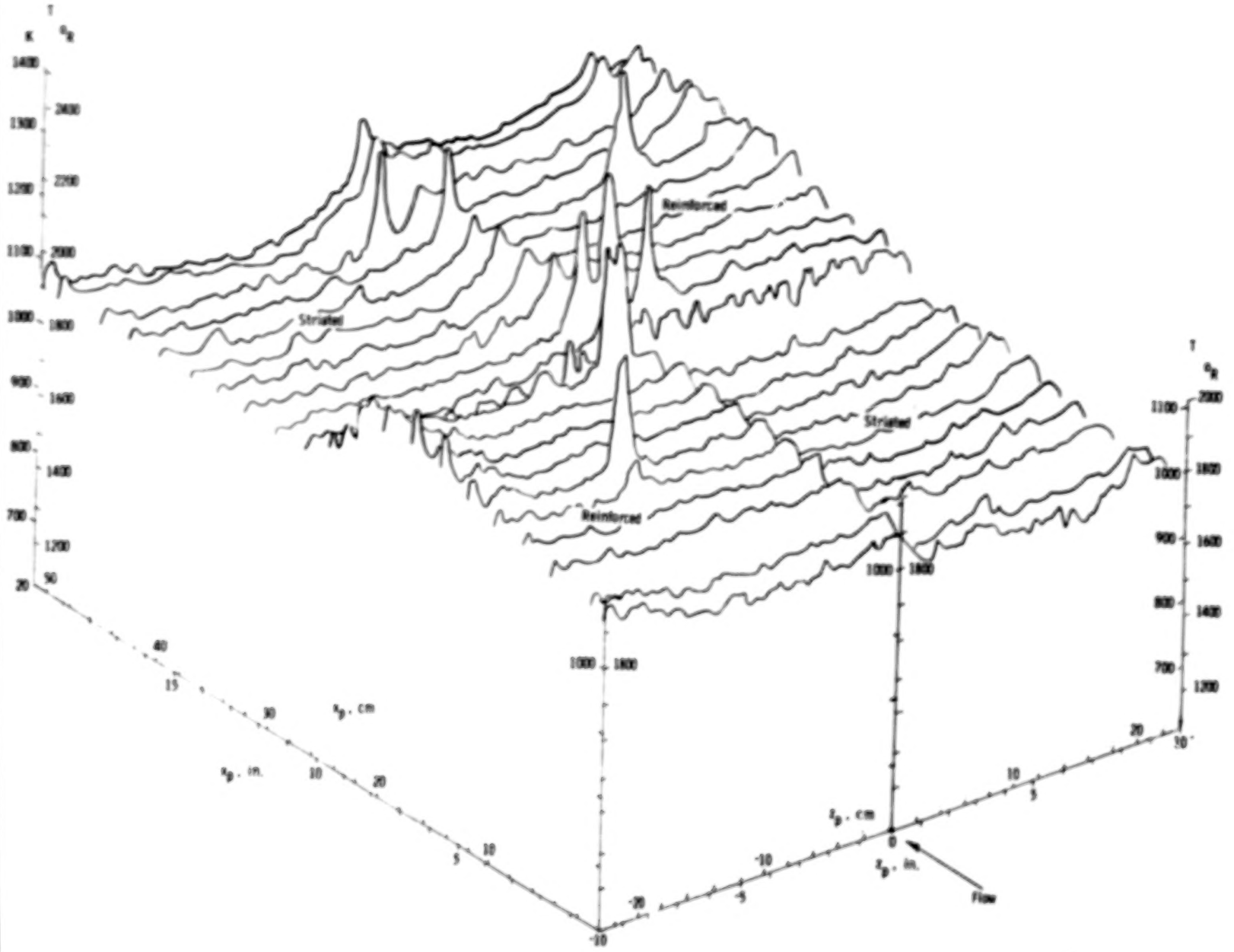

Figure 17.- Surface-temperature relief map of panel 2 during test 8.

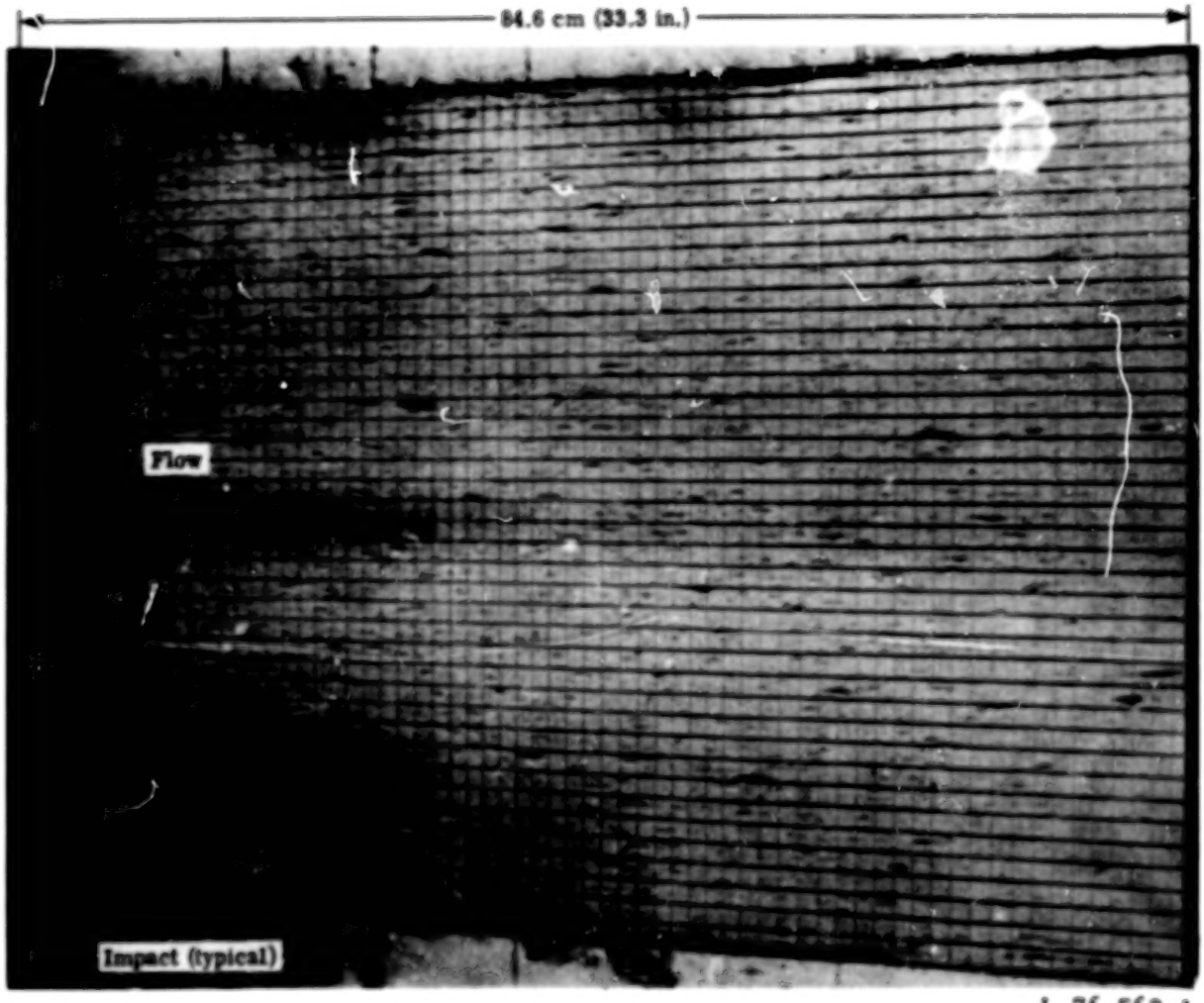

L-76-562.1

Figure 18.- Panel 3 after test 6.

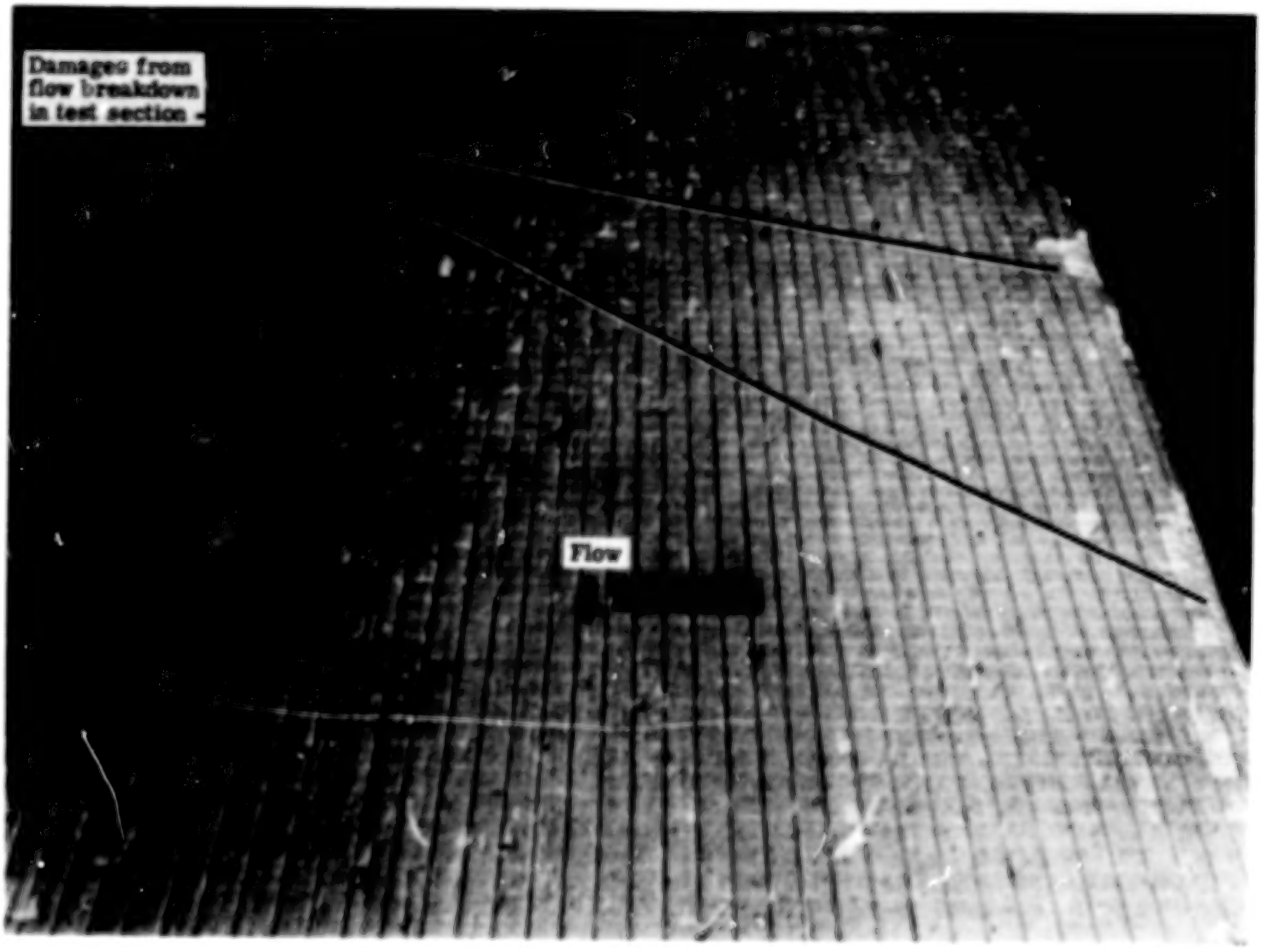

L-76-729.1

Figure 19.- Panel 3 after test 7.

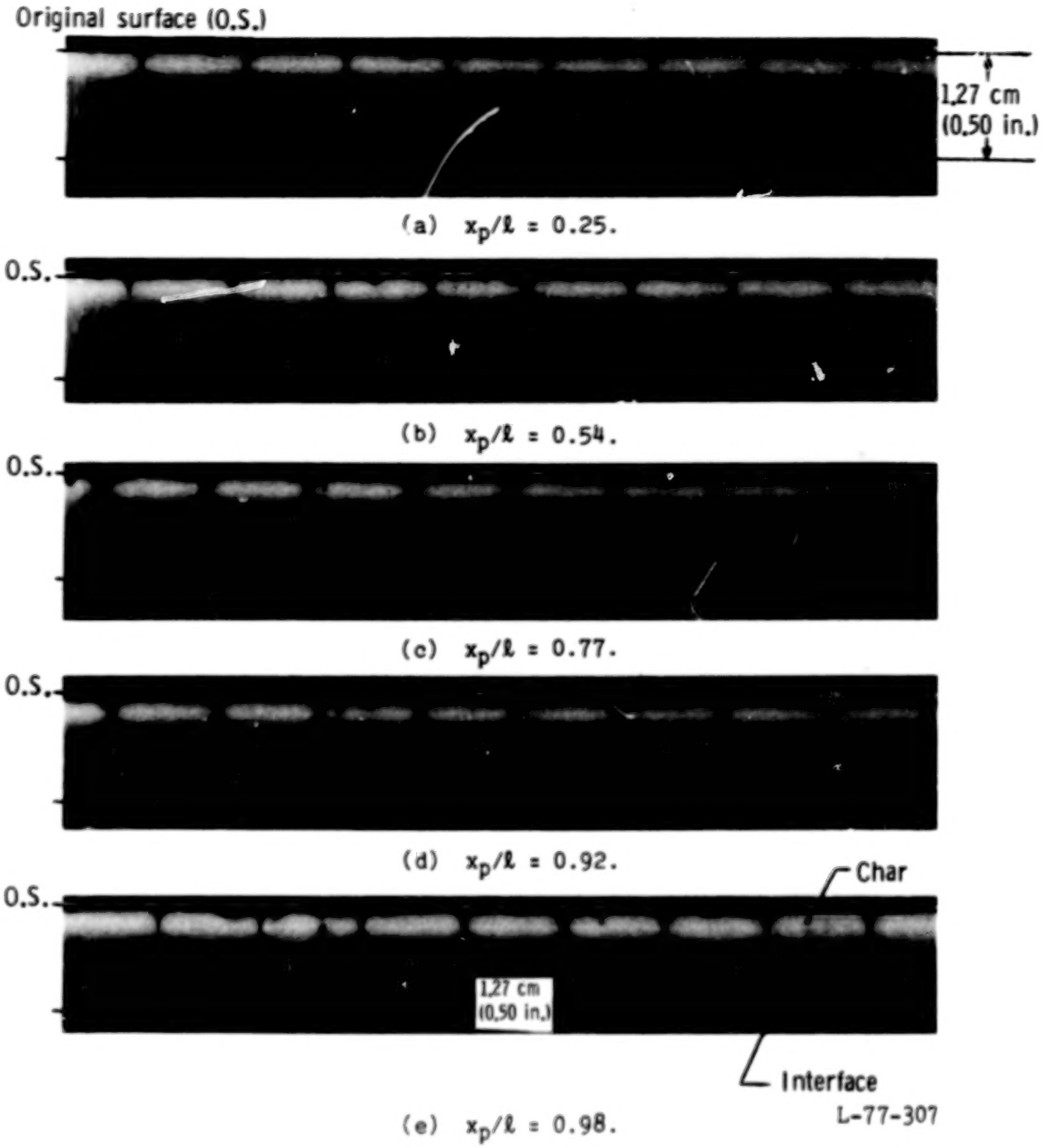

Figure 20.- Spanwise-section photographs of panel 3. ℓ = 84.6 cm (33.3 in.).

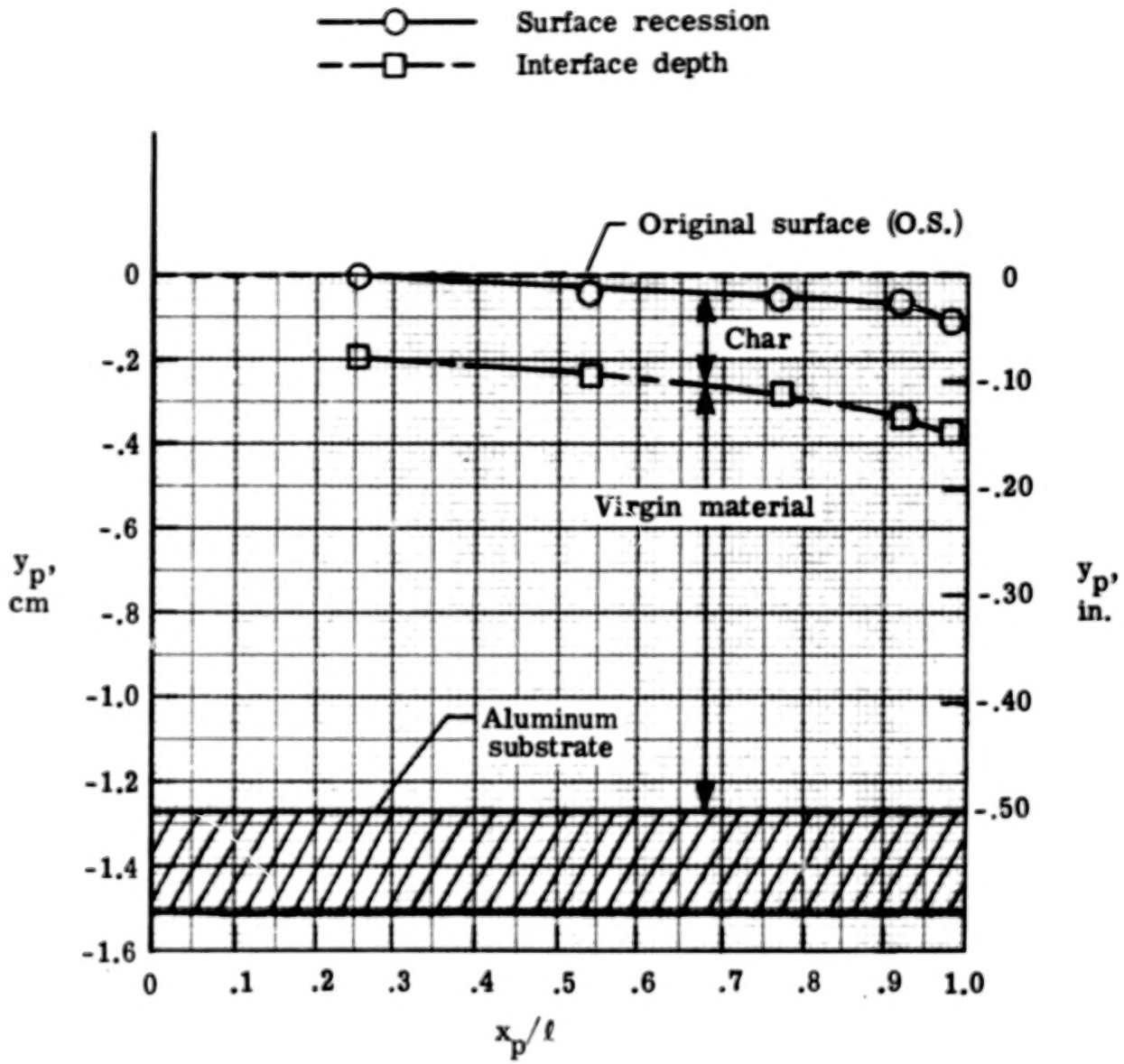

Figure 21.- Distribution of surface recession and char–virgin-material interface depth for panel 3 after test completion.

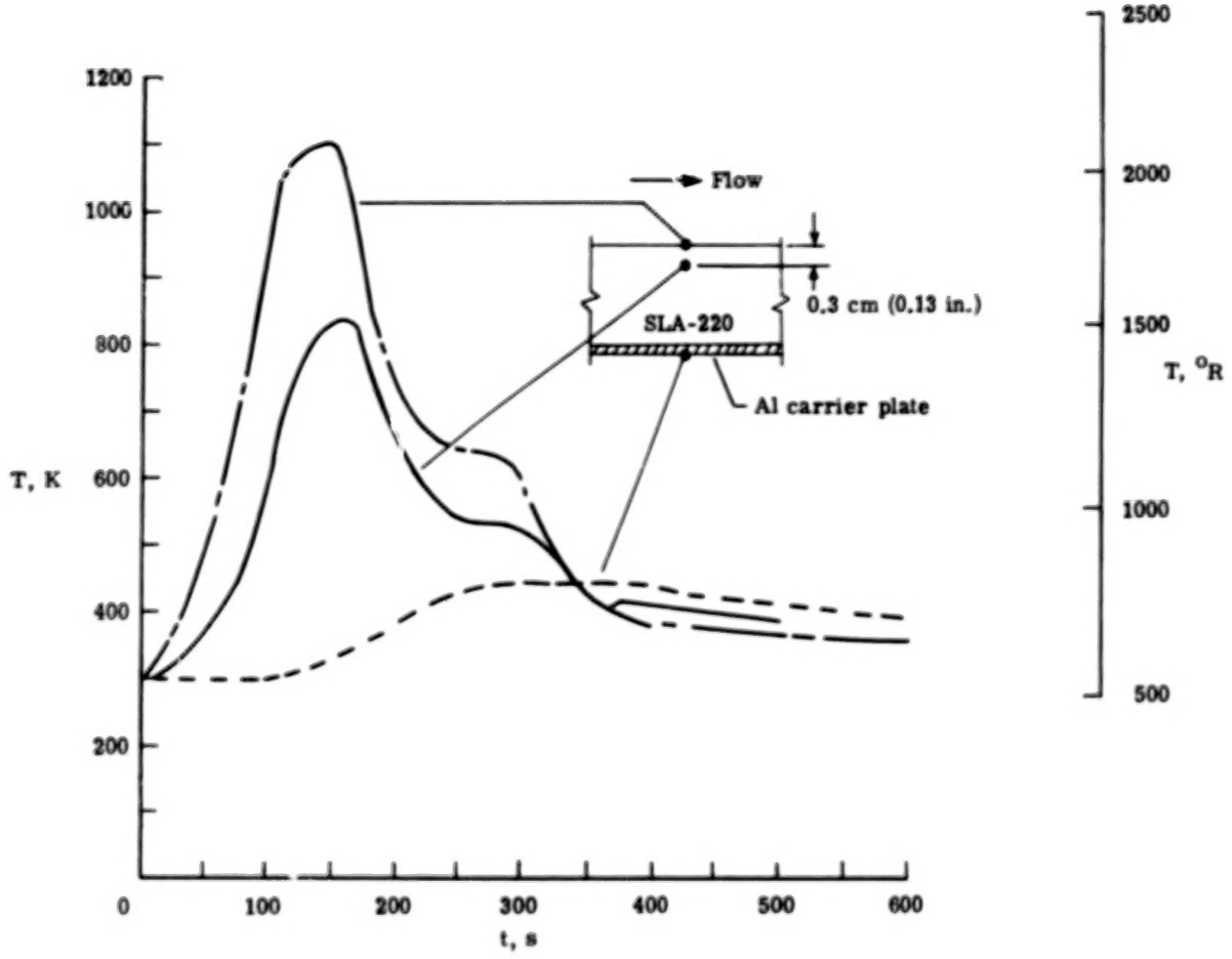

Figure 22.- Temperature history of panel 2 during radiant heating test.

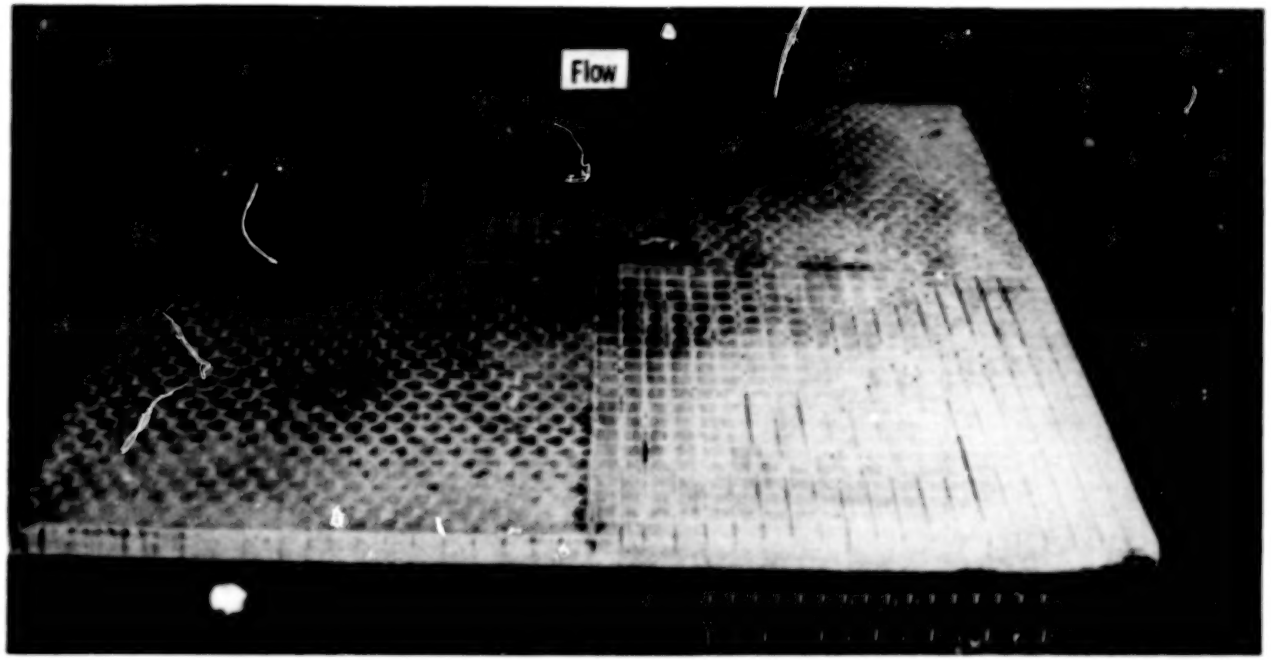

L-76-2722.1

Figure 23.- Test panel 2 after exposure to excessive heat of radiant heating cycle.

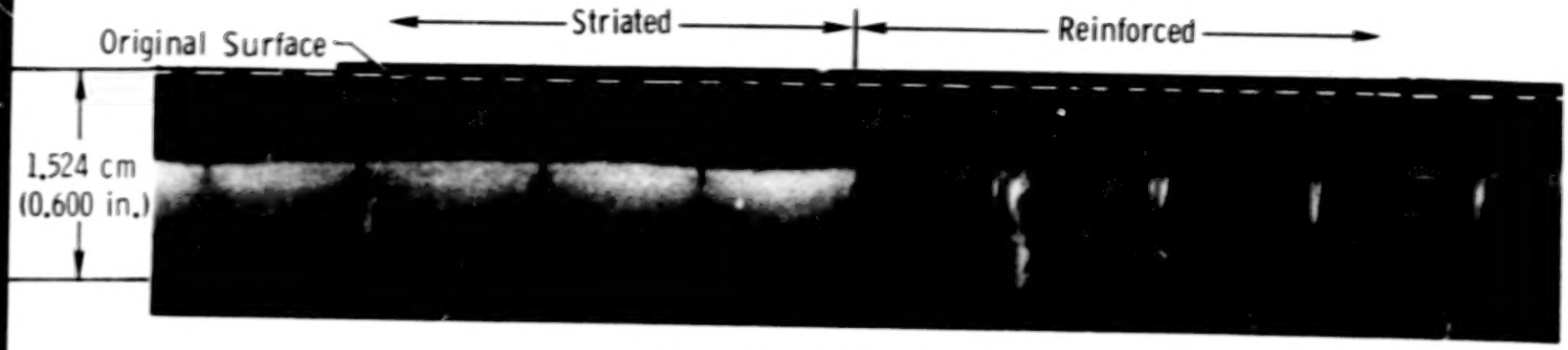

(a) $x_p/\ell = 0.063$.

L-77-308

(b) $x_p/\ell = 0.94$.

Figure 24.- Spanwise-section photographs of test panel 2. ℓ = 50.8 cm (20.0 in.).

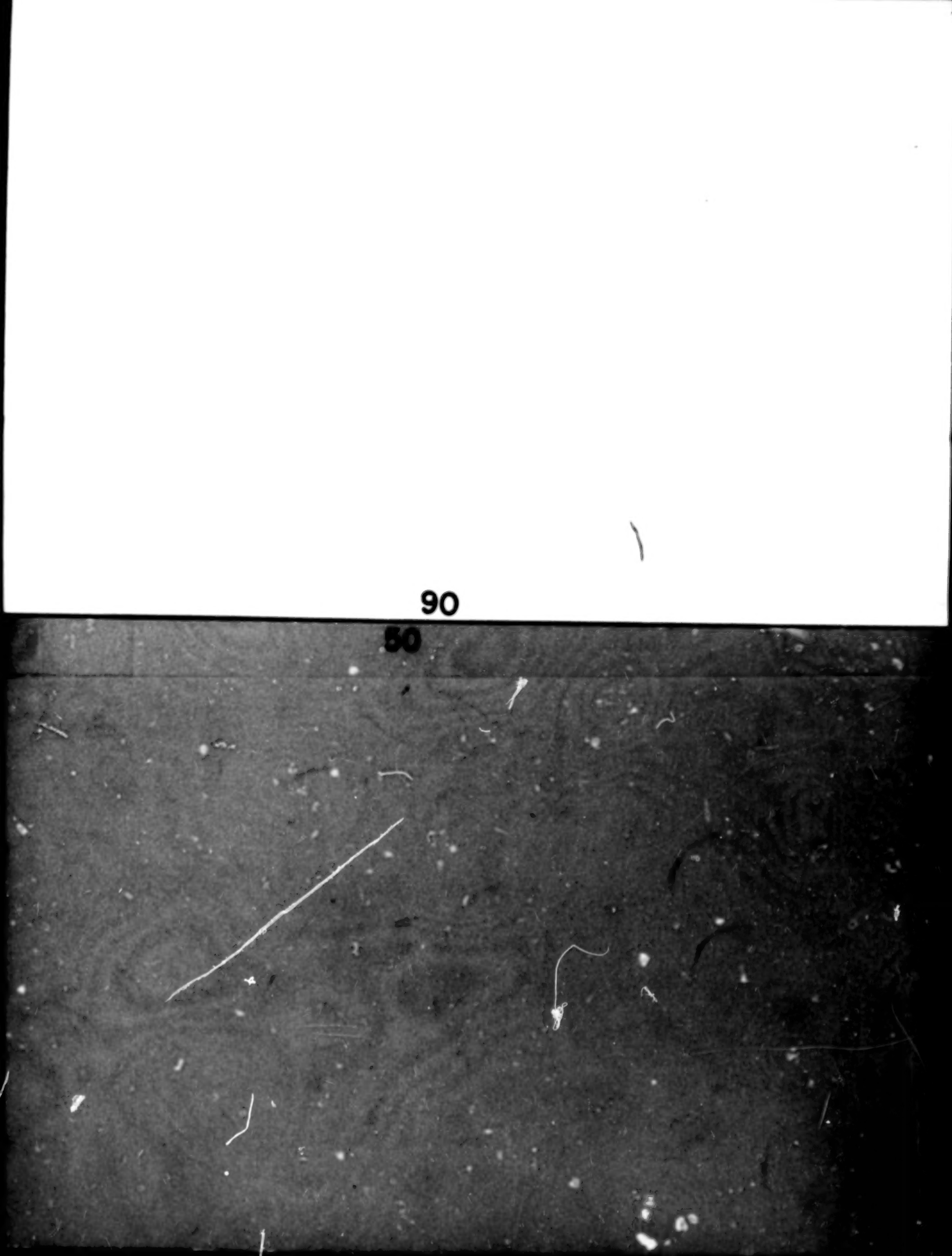
90
50

END

5.2278